

# Improving Neuron-level Interpretability with White-box Language Models

Hao Bai<sup>1,2</sup> Yi Ma<sup>1,3</sup>

<sup>1</sup>UC Berkeley <sup>2</sup>UIUC <sup>3</sup>HKU

<https://crate-lm.github.io/>

Neurons in auto-regressive language models like GPT-2 can be interpreted by analyzing their activation patterns. Recent studies have shown that techniques such as dictionary learning, a form of post-hoc sparse coding, enhance this neuron-level interpretability. In our research, we are driven by the goal to fundamentally improve neural network interpretability by embedding sparse coding directly within the model architecture, rather than applying it as an afterthought. In our study, we introduce a white-box transformer-like architecture named Coding RAtE TransformEr (CRATE), explicitly engineered to capture sparse, low-dimensional structures within data distributions. Our comprehensive experiments showcase significant improvements (up to 103% relative improvement) in neuron-level interpretability across a variety of evaluation metrics. Detailed investigations confirm that this enhanced interpretability is steady across different layers irrespective of the model size, underlining CRATE’s robust performance in enhancing neural network interpretability. Further analysis shows that CRATE’s increased interpretability comes from its enhanced ability to consistently and distinctively activate on relevant tokens. These findings point towards a promising direction for creating white-box foundation models that excel in neuron-level interpretation.

## 1. Introduction

*Representation learning* aims to learn a continuous mapping, to transform a random vector in a high dimensional space that is sampled from a dataset, to a feature vector in another (typically lower-dimensional) space [1]. Recently, deep learning has witnessed tremendous empirical success in modeling massive amounts of high-dimensional data, and the predominant practice has been to learn first a task-agnostic representation by pre-training a large neural network, which is commonly known as the *foundation model* [2, 3]. Among language foundation models, the transformers architecture [4] with Generative Pre-Training [3] (GPT) has recently demonstrated a strong capability of modeling sequential data and thus predicting subsequent tokens [5, 6]. Such strong capability has emerged significant success in downstream applications [7, 8], yet the large neural network is known to be *black-box*, where the representations in the model are not independently interpretable, introducing difficulty in designing effective paradigms for major known challenges of (visual) language models like hallucination [9, 10], bias [11, 12], and catastrophic forgetting [13, 14].

To interpret the functions of individual modules in the language models, *mechanistic interpretation* was proposed to reverse-engineer such models, through identifying meaningful patterns in the data representations and computational mechanisms of the model components [15, 16]. Recent studies on auto-regressive models like GPT-2 have delved into *neuron-level interpretation*, where the focus is on understanding the activations within the model’s MLP layers [17]. This approach helps to reveal the specific roles of individual neurons, which is crucial for precise model editing and control [16, 18]. Recent research has also proposed that *sparse auto-encoder* (SAE)-based dictionary learning effectively promotes mono-semanticity of neurons, thus enhancing neuron-level

---

This work was entirely done at UC Berkeley.



Figure 1: Instances are systematically identified where the interpretability of CRATE (ours, row 1) outperforms GPT-2 (row 2). For each neuron (rounded box), we show two top activated text excerpts (excerpt 1 and 2) and one randomly activated excerpt (excerpt 3). Results show that CRATE consistently activates on and only on semantically relevant text excerpts (first two excerpts), leading to more precise explanations predicted by agents like Mistral.

interpretability [19]. However, as a post-hoc method, sparse auto-encoders introduce non-negative reconstruction loss, causing noise and reducing fidelity when interpreting neurons [19]. Recent studies also highlight their scalability challenges, as neuron decomposition becomes difficult in larger language models due to the vast number of directions [20–22].

*Can we instead build sparsity directly into the language model?* In this paper, we develop the CRATE language model, a GPT-2-size language model that builds sparse coding into the model with a mathematically principled way. CRATE handles the problems introduced by sparse encoders at scale: it (i) escapes the loss introduced in reconstructing the language model representations, enabling loss-free steering, and (ii) escapes the unsteady process of training a sparse auto-encoder. To avoid adding inconsistency into the language model, we develop on top of a mathematically principled white-box model framework, named CRATE [23].<sup>1</sup> After encoding the text tokens into numbers, we apply language-domain-specific modifications to the original CRATE architecture and obtain the token representations. The final representations are then used to predict the next token, while the intermediate representations gets interpreted.

To this end, the main contribution of this work is to propose a causal language model architecture based on the CRATE model framework that builds sparsity inherently, that achieves significantly better neuron-level interpretability (up to **103% relative increase**) than language models with the GPT-2 architecture under a similar configuration. CRATE forms a family of models from single-layer model up to a 12-layer configuration. Comparative qualitative analysis of neuron activations between CRATE and GPT-2 is provided in Figure 1, alongside extensive quantitative evaluations demonstrating that *by explicitly integrating sparse coding into the language model, CRATE achieves markedly improved interpretability across layers compared to GPT-2, applicable across a wide range of model sizes under a variety of evaluation metrics.*

<sup>1</sup>In the remaining parts of the paper, we use “CRATE” or “CRATE language model” to refer to our language model architecture, while “original CRATE” denotes the architecture framework described in the literature.

## 2. Related Work

**Neuron-level interpretation.** Recent studies have provided insights into how auto-regressive models like GPT-2 work at the level of individual neurons, named *neuron-level interpretation*. These studies focus on analyzing *activations*, which are the outputs from the activation functions within the model’s multi-layer perceptron (MLP) blocks [17]. Neuron-level interpretation is crucial to understanding the mechanisms in a model, including what concepts are learned in the neurons of the network, whether specific neurons are learning particular concepts, and how localized/distributed and redundantly the knowledge is preserved within neurons of the network.

A higher neuron-level interpretability indicates that more neurons are interpretable or neurons are more interpretable [24]. As interpretations of the neurons can help localize the knowledge obtained in a neural network, neuron-level interpretation can be used for editing the knowledge in models [16, 18], model pruning and distillation [25], adapting the model to different domains and steering the output [26, 27], and debugging model errors [28]. Improved neuron-level interpretability increases reliability and performance in the applications above.

**Sparse auto-encoders.** To enhance interpretability, post-hoc sparse coding methods like dictionary learning [29] are used, but these techniques result in imperfect reconstructions and thus always introduces loss when steering the model [19, 30]. Literature also indicates that sparse-autoencoders are hard to scale, i.e., a dramatic drop in the number of interpretable features can be observed when the model being interpreted becomes deeper [20]. Additionally, tuning SAE models for larger  $L$  values involves extensive hyperparameter tuning and time-consuming training, requiring multiple metrics (reconstruction rate, L1 loss, number of dead neurons) for reliable judgment, which can’t be easily optimized with automatic engineering tricks [19].

**Evaluation of neuron-level interpretability.** Metrics now exist to evaluate neuron-level interpretability in language models, examining if neurons trigger on relevant tokens in given contexts [19, 31]. Recent works have demonstrated that a small number of circuits in language models are interpretable [32, 33], but comprehending each neuron, out of millions, is vital for thorough model safety audits. Given the prohibitive cost of human evaluation on such a scale, OpenAI introduced an automated metric using large language models for interpretability assessment [31], which Anthropic later refined for sparse activations [19]. These methods align closely with human judgment and have gained broad acceptance within the research community [34–37]. These metrics show that neuron-level interpretability in auto-regressive models is limited [24], where the popular hypothesis is that neurons are superpositions of simpler semantics, which makes them *fire* (produce a high activation) at multiple semantically distinct sets of tokens [38]. Metrics mentioned above are what we use in this work.

**White-box models and structured representation learning.** In the domain of structured representation learning, *white-box* models stand out for their ability to generate explicit, structured data representations that adhere to specific, desirable configurations such as sparsity and piece-wise linearity, as discussed by Gregor and LeCun [39] and Chan et al. [40]. Within this framework, Yu et al. [23] introduced an innovative approach to constructing deep networks based on unrolled optimization. Specifically, Yu et al. [23] proposed the `CRATE` foundation model framework, utilizing an information-theoretic objective aimed at promoting the *compression and sparsity* of data towards a predefined statistical structure. Recently, empirical experiments suggest that the white-box design of `CRATE` inherently develops segmentation capabilities from the data representations at both holistic and component levels with supervised training in the vision domain [41], which directly motivates us to further explore the data representations within such architecture for language models. Recent work has also shown that the `CRATE` framework is scalable: it can be effectively scaled up to comparable performance as Vision Transformer (ViT) with careful engineering [42]. Furthermore, the fine-tuning performance of the pretrained `CRATE` model is also proven to be comparable in both the language domain [23] and vision domain [42].

### 3. Preliminaries on the CRATE Architecture

This section introduces the original `CRATE` architecture introduced in Yu et al. [23].

**Notations.** In this paper, we denote the one-hot input tokens by  $\mathbf{X} = [\mathbf{x}_1, \dots, \mathbf{x}_N] \in \mathbb{R}^{V \times N}$ , where  $\mathbf{x}_i \in \mathbb{R}^{V \times 1}$  represents the  $i$ -th one-hot token,  $N$  is the total number of input tokens, and  $V$  is the vocabulary size. We use  $f \in \mathcal{F} : \mathbb{R}^{V \times N} \rightarrow \mathbb{R}^{d \times N}$  to denote the mapping induced by the model, which is a composition of  $L + 1$  operators (layers)  $f = f^L \circ \dots \circ f^\ell \circ \dots \circ f^1 \circ f^{\text{pre}}$ , where  $f^\ell : \mathbb{R}^{d \times N} \rightarrow \mathbb{R}^{d \times N}$  ( $1 \leq \ell \leq L$ ) represents the mapping of the  $\ell$ -th operator, and  $f^{\text{pre}} : \mathbf{X} \in \mathbb{R}^{V \times N} \rightarrow \mathbf{Z}^1 \in \mathbb{R}^{d \times N}$  represents the pre-processing layer that transforms the one-hot token representations  $\mathbf{X} = [\mathbf{x}_1, \dots, \mathbf{x}_N]$  to semantic embeddings  $\mathbf{Z}^1 = [z_1^1, \dots, z_N^1]$ . We let  $\mathbf{Z}^\ell$  denote the input token representations of the  $\ell$ -th operator  $f^\ell$  for  $1 \leq \ell \leq L$ , so that  $z_i^\ell \in \mathbb{R}^d$  denotes the representation of the  $i$ -th token  $\mathbf{x}_i$  before the  $\ell$ -th layer. We denote  $\mathbf{Z} = \mathbf{Z}^{L+1}$  as the output token representations of the last ( $L$ -th) layer.

**Framework, objective, and optimization.** The transformation of input data into *parsimonious* (piecewise linearized and compact) representations is accomplished by adopting a local signal model for the marginal distribution of the tokens  $z_i$ . This statement suggests that the tokens can be approximately considered to occupy a union of several (identified as  $K$ ) low-dimensional spaces, each with a dimension  $p \ll d$ . These spaces are characterized by orthonormal bases, represented as  $\mathbf{U}_{[K]} = (\mathbf{U}_k)_{k=1}^K$  where  $\mathbf{U}_k \in \mathbb{R}^{d \times p}$ . Within the framework of this local signal model, `CRATE` aims to optimize the *sparse rate reduction* objective:

$$\max_{f \in \mathcal{F}} \mathbb{E}_{\mathbf{Z}} [\Delta R(\mathbf{Z} | \mathbf{U}_{[K]}) - \lambda \|\mathbf{Z}\|_0] = \max_{f \in \mathcal{F}} \mathbb{E}_{\mathbf{Z}} [R(\mathbf{Z}) - \lambda \|\mathbf{Z}\|_0 - R^c(\mathbf{Z}; \mathbf{U}_{[K]})]. \quad (1)$$

where  $\lambda$  is the sparsification regularizer and  $\mathbf{Z} = f(\mathbf{X})$ . The coding rate  $R(\mathbf{Z})$  serves as a close estimate (following Ma et al. [43]) for the average amount of bits necessary for encoding the tokens  $z_i$  to a precision level  $\varepsilon$  using a Gaussian codebook. Additionally,  $R^c(\mathbf{Z} | \mathbf{U}_{[K]})$  represents the theoretical maximum average amount of bits needed to encode the projection of the tokens onto each low dimensional subspace defined in the local signal model, specifically  $\mathbf{U}_k^* z_i$ , to the same precision level  $\varepsilon$  utilizing a Gaussian codebook, as outlined by Yu et al. [23]. If the subspaces are adequately incoherent from each other, the solutions that minimize the object function, viz. Equation (1), in terms of  $\mathbf{Z}$ , are associated with subspace configurations that are both incoherent and aligned with the axes, as pointed out by Yu et al. [44].

A network aimed at optimizing the sparse coding rate reduction objective through unrolled optimization gradually shifts the distribution of  $\mathbf{X}$  towards the intended canonical forms, where each iteration of the unrolled optimization process acts as a layer:

$$f : \mathbf{X} \xrightarrow{f^{\text{pre}}} \mathbf{Z}^1 \rightarrow \dots \rightarrow \mathbf{Z}^\ell \xrightarrow{f^\ell} \mathbf{Z}^{\ell+1} \rightarrow \dots \rightarrow \mathbf{Z}^{L+1} = \mathbf{Z}. \quad (2)$$

The iterative optimization framework incorporates multiple design choices, among which is a two-step alternating minimization approach grounded in robust theoretical principles [23]. This approach delineates two distinct blocks: the `MSSA` and the `ISTA` block, collectively defining a single `CRATE` layer:

$$\mathbf{Z}^{\ell+1/2} \doteq \mathbf{Z}^\ell + \text{MSSA}(\mathbf{Z}^\ell | \mathbf{U}_{[K]}^\ell), \quad f^\ell(\mathbf{Z}^\ell) = \mathbf{Z}^{\ell+1} \doteq \text{ISTA}(\mathbf{Z}^{\ell+1/2} | \mathbf{D}^\ell). \quad (3)$$

**Compression operator: Multi-Head Subspace Self-Attention (MSSA).** Given local models  $\mathbf{U}_{[K]}^\ell$ , to form the incremental transformation  $f^\ell$  optimizing Equation (1) at layer  $\ell$ , `CRATE` first compresses the token set  $\mathbf{Z}^\ell$  against the subspaces by minimizing the coding rate  $R^c(\cdot | \mathbf{U}_{[K]}^\ell)$ . As Yu et al. [23] show, doing this minimization locally by performing a step of gradient descent on  $R^c(\cdot | \mathbf{U}_{[K]}^\ell)$  leads to the so-called multi-head subspace self-attention (MSSA) operation, defined as



$$\text{MSSA}(\mathbf{Z} \mid \mathbf{U}_{[K]}) \doteq \frac{p}{(N+1)\varepsilon^2} [\mathbf{U}_1, \dots, \mathbf{U}_K] \begin{bmatrix} (\mathbf{U}_1^* \mathbf{Z}) \text{softmax}((\mathbf{U}_1^* \mathbf{Z})^* (\mathbf{U}_1^* \mathbf{Z})) \\ \vdots \\ (\mathbf{U}_K^* \mathbf{Z}) \text{softmax}((\mathbf{U}_K^* \mathbf{Z})^* (\mathbf{U}_K^* \mathbf{Z})) \end{bmatrix}, \quad (4)$$

In practice, the calculation of the intermediate representations  $\mathbf{Z}^{\ell+1/2}$  with the output from the MSSA block is calculated in a weighted form:

$$\mathbf{Z}^{\ell+1/2} \approx \left(1 - \kappa \cdot \frac{p}{(N+1)\varepsilon^2}\right) \mathbf{Z}^\ell + \kappa \cdot \frac{p}{(N+1)\varepsilon^2} \cdot \text{MSSA}(\mathbf{Z}^\ell \mid \mathbf{U}_{[K]}), \quad (5)$$

where  $\kappa > 0$  is a learning rate hyperparameter. This block resembles to the multi-head self-attention block of the GPT-2 model, but the query, key, and value projection matrices within a single head are all identical in the MSSA block.

**Sparsification operator: Iterative Shrinkage-Thresholding Algorithm (ISTA).** The remaining term to optimize in Equation (1) is the difference of the global coding rate  $R(\mathbf{Z})$  and the  $\ell^0$  norm of the tokens, which together encourage the representations to be both sparse and non-collapsed. Yu et al. [23] show that local minimization of this objective in a neighborhood of the intermediate representations  $\mathbf{Z}^{\ell+1/2}$  is approximately achieved by a LASSO problem with respect to a sparsifying orthogonal dictionary  $\mathbf{D}^\ell \in \mathbb{R}^{d \times h}$ . Taking an iterative step towards solving this LASSO problem gives the iterative shrinkage-thresholding algorithm (ISTA) block [23, 45]. The ReLU non-linearity appearing in this block arises from an additional non-negativity constraint on the representations in the LASSO program, motivated by the goal of better separating distinct modes of variability in the token distribution:

$$\mathbf{Z}^{\ell+1} = f^\ell(\mathbf{Z}^\ell) = \text{ReLU}(\mathbf{Z}^{\ell+1/2} + \eta \mathbf{D}^{\ell*} (\mathbf{Z}^{\ell+1/2} - \mathbf{D}^\ell \mathbf{Z}^{\ell+1/2}) - \eta \lambda \mathbf{1}) \doteq \text{ISTA}(\mathbf{Z}^{\ell+1/2} \mid \mathbf{D}^\ell). \quad (6)$$

## 4. The CRATE Language Model

This section introduces the difference between our work and the original CRATE paper [23], thus introducing what changes we made to the CRATE architecture.

First, we note that the task in this work is different: we apply the CRATE architecture to the *next-token prediction task* in the language domain, while the original CRATE paper applies the architecture to the image classification task in the vision domain. This difference immediately leads to differences when designing the model architecture: (i) we apply a causal mask to the original CRATE model to avoid the model seeing tokens after the current token, and (ii) we change the embedding layer and heads of the original CRATE model to fit the language vocabulary.

Second, we’re interested in interpreting the neurons within CRATE on the next-token prediction task and making *direct comparisons* to the GPT-2 model architecture. As neuron-level interpretation is commonly evaluated on the hidden states in the MLP block of the GPT-2 model [19, 31], (iii) we *over-parameterize* (increase the hidden dimension of) the ISTA block of the original CRATE model to align with the hidden dimension of the MLP block of the GPT-2 model.

Below we show specific definitions of the modifications we made. We illustrate the architecture in Figure 2, and show implementation details in Appendix A.

**Embedding and Head.** In order to apply the CRATE architecture to the language domain, we define the pre-processing layer  $f^{\text{pre}}$  that transforms language tokens into position-aware semantic embeddings, and define post-processing head  $f^{\text{head}}(\mathbf{Z})$  that maps the final representations to output token distributions in the vocabulary space:

$$f^{\text{pre}}(\mathbf{X}) = \mathbf{E}_{\text{sem}}(\mathbf{X}) + \mathbf{E}_{\text{pos}}, \quad f^{\text{head}}(\mathbf{Z}) = \mathbf{W}^{\text{head}} \mathbf{Z}, \quad (7)$$

where  $\mathbf{E}_{\text{sem}}$  is a semantic embedding matrix that maps input tokens  $x_i$  to embedding vectors in  $\mathbb{R}^d$ ,  $\mathbf{E}_{\text{pos}} \in \mathbb{R}^{d \times N}$  is a positional embedding matrix, and  $\mathbf{W}^{\text{head}} \in \mathbb{R}^{V \times d}$  maps the (contextualized)

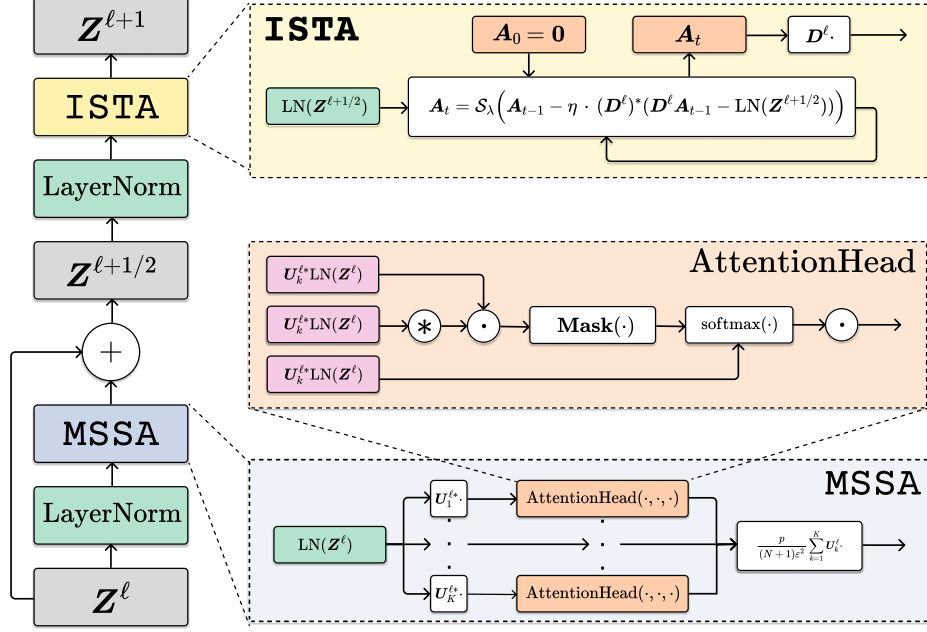


Figure 2: Block architecture for the CRATE language model, where  $S_\lambda(x) = \text{ReLU}(x - \eta \cdot \lambda \cdot 1)$ . Differences from the original architecture mentioned in Yu et al. [23] are marked **bold**: we (i) add a causal mask  $\text{Mask}(\cdot)$  and (ii) over-parameterize the ISTA block.

token representations  $\mathbf{Z}^{L+1}$  to the distribution of the next token. All parameters mentioned above are learnable.

**MSSA Block.** To align with the next word prediction task used in GPT-2 [3], we replace the attention matrix in MSSA (Equation (4)) with a *causally masked* self-attention, defined as

$$\begin{aligned} \text{softmax}((\mathbf{U}_k^* \mathbf{Z})^* (\mathbf{U}_k^* \mathbf{Z})) &\rightarrow \text{softmax}(\text{CausalMask}((\mathbf{U}_k^* \mathbf{Z})^* (\mathbf{U}_k^* \mathbf{Z}))), \\ \text{where } \text{CausalMask}(M)_{ij} &= \begin{cases} M_{ij}, & i \leq j \\ -\infty, & i > j. \end{cases} \end{aligned} \quad (8)$$

**ISTA Block.** To investigate the neuron interpretability of the activation matrix  $\mathbf{A} \in \mathbb{R}^{h \times N}$ , we design an *overcomplete* version of the original ISTA block (Equation (6)) with  $\mathbf{D}^\ell \in \mathbb{R}^{d \times h}$  where  $h = nd$ , and  $n = 4$  to keep a fair comparison to the GPT-2 [3] and standard transformer architecture Vaswani et al. [4]):

$$\begin{aligned} \mathbf{A}_t &\doteq \text{ISTA}(\mathbf{Z}^{\ell+1/2} \mid \mathbf{D}^\ell), \\ \mathbf{A}_k &= \text{ReLU}(\mathbf{A}_{k-1} - \eta (\mathbf{D}^\ell)^* (\mathbf{D}^\ell \mathbf{A}_{k-1} - \mathbf{Z}) - \eta \cdot \lambda \cdot \mathbf{1}), \quad \mathbf{A}_0 = \mathbf{0}, \quad k \in [t], \\ \mathbf{Z}^{\ell+1} &= \mathbf{D}^\ell \mathbf{A}_t, \end{aligned} \quad (9)$$

where  $\eta > 0$  is the step size,  $\lambda > 0$  is the sparsification regularizer, and  $t$  is the number of ISTA iterations. In practice, we set  $t = 2$  to keep computation efficient. The ISTA block resembles the MLP block in the GPT-2 model, but with a relocated skip connection.

**Token Processing.** The desired token processing procedure is illustrated in Figure 3. The process starts with random token representations ( $\mathbf{Z}^1$ ). Through successive layers, the representations ( $\mathbf{Z}^\ell$ ) are *compressed* to align with the axis via the MSSA block, forming  $\mathbf{Z}^{\ell+1/2}$  that are semantically more consistent among relevant tokens. This is then refined by *sparse coding* (the ISTA block) to produce the representations  $\mathbf{Z}^{\ell+1}$  that align on incoherent axes, leading to semantically more specified token representations. Repeated across layers, this culminates in distinct token representations  $\mathbf{Z}^{L+1}$  aligned on unique semantic axes. More detailed explanation of this optimization process can be found in Appendix A.4.

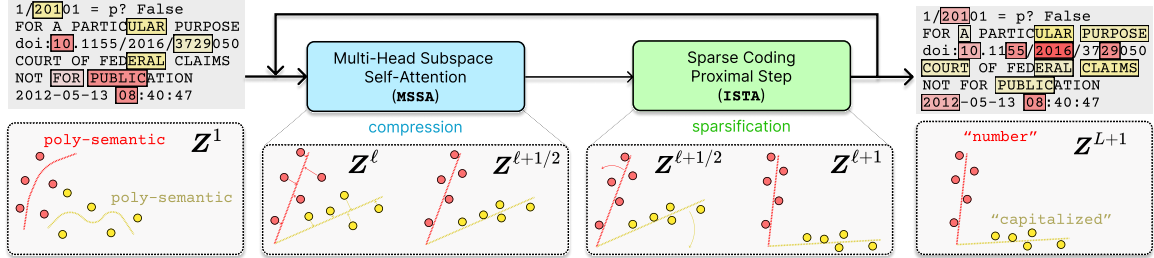


Figure 3: CRATE iteratively compresses (MSSA block) and sparsifies (ISTA block) the token representations (*colored points*) across its layers from 1 to  $L$ , transforming them into parsimonious representations aligned on axes (*colored lines*) with distinct semantic meanings.

## 5. Empirical Experiments

We examine the next token prediction performance and neuron interpretability of CRATE in this section. We detail the architecture, size, pre-training recipe (Section 5.1), performance (Section 5.2), and neuron-level interpretability (Section 5.3) of CRATE compared to the standard transformer architecture. In this section, we denote  $K$  as the number of attention heads,  $d$  as the dimension of the residual stream in the model, and  $h$  as the hidden (inner) dimension of the ISTA or MLP module.

### 5.1. Setup

**Model architecture and size.** The CRATE model is designed with various sizes  $L \in \{1, 2, 3, 6, 12\}$ , where each size matches the GPT-2 configurations for direct comparisons, as shown in Section 5.1. Configurations for  $L \in \{1, 2, 3\}$  adhere to GPT-2 models as per Bricken et al. [19], while  $L \in \{6, 12\}$  follow configurations from Sanh et al. [46] and Radford et al. [3], respectively. Notably, CRATE maintains approximately 2/3 the size of GPT-2 at scale. Both models utilize the Byte-level BPE tokenizer with a vocabulary size of 50,257, following Radford et al. [3]. We explain the parameter size difference between CRATE and GPT-2 in Appendix A.1.

Model Config	$d$	$K$	$L$	$h$	CRATE	GPT-2
1L	128	4	1	512	6.54M	6.64M
2L	128	4	2	512	6.64M	6.83M
3L	128	4	3	512	6.74M	7.03M
S(mall)	768	12	6	3,072	55.9M	81.1M
B(ase)	768	12	12	3,072	81.2M	123.6M

Table 1: Model configuration of CRATE and model size comparison to GPT-2.

**Datasets and optimization.** We pre-train both models on the next token prediction task using the uncopyrighted *Pile* dataset [47] and the Adam optimizer [48]. Following Bricken et al. [19], we pre-train both CRATE and GPT-2 of smaller sizes ( $L \in \{1, 2, 3\}$ ) on 100 billion tokens with a context window of 1,024 tokens. Following the pre-training setup in Karpathy [49] and scaling law in Touvron et al. [50], we pre-train using 100 billion tokens for the Small models, and 160 billion tokens for the Base models.<sup>2</sup> It takes about 4 days to pre-train CRATE-Base on 160 billion tokens with 32 A5000 GPUs.

### 5.2. Performance

This section demonstrates that CRATE, despite not outperforming GPT-2, still generates reasonable predictions, as evidenced through quantitative and qualitative comparisons.

We observe that both training and validation loss curve of CRATE-Base on the *Pile* dataset converges well, as presented in Figure 4 (*left*). Although the convergence is slower than GPT-2, the loss curve of CRATE keeps decreasing after training on 160 billion tokens, while GPT-2 already tends to converge.

<sup>2</sup>Practically, we train with a batch size of 768 for 125,000 iterations for  $L \in \{1, 2, 3, 6\}$ , and a batch size of 256 for 600,000 iterations for  $L = 12$ .

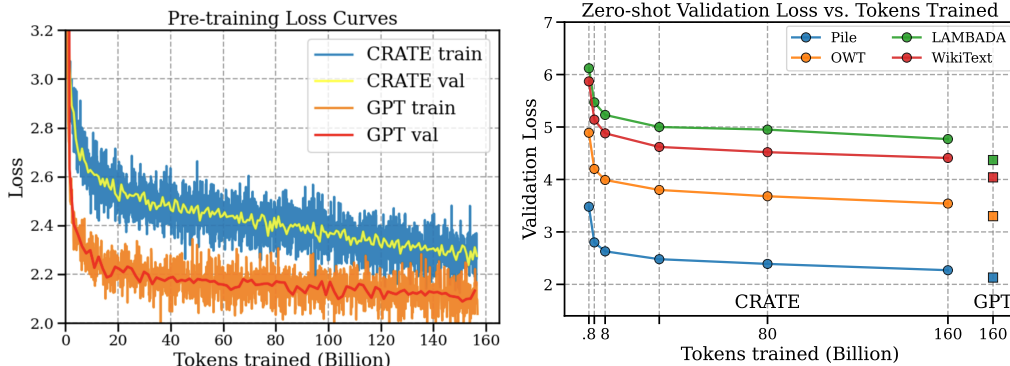


Figure 4: *Left*: loss curve when pre-training CRATE-Base and GPT2-Base on the Pile dataset. *Right*: zero-shot validation loss of CRATE evaluated on a variety of datasets (Pile, LAMBADA, OpenWebText and WikiText).

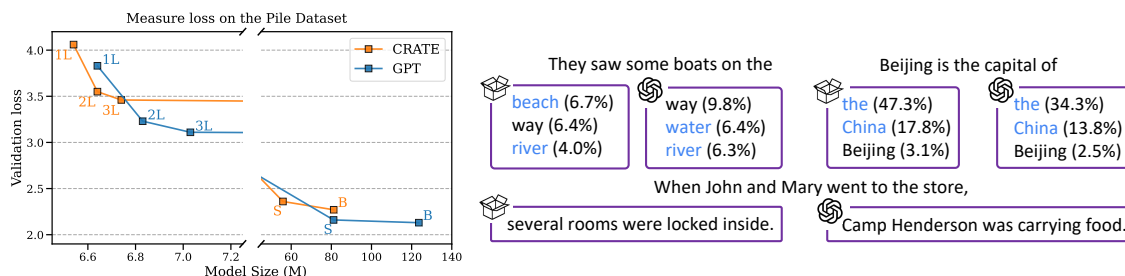


Figure 5: *Left*: Validation loss of CRATE compared to GPT-2 on the Pile dataset, with respect to the model size. *Right*: Qualitative examples of predictions made by CRATE and GPT-2. The tokens in blue are considered good. We compare CRATE-Base to GPT2-Base on the next word prediction task.

We also demonstrate the zero-shot validation loss curve of CRATE evaluated on OpenWebText as well as other datasets [3] in Figure 4 (*right*). Results show that CRATE effectively learns transferable representations across a number of datasets, and achieves comparable performance to GPT-2 after full training on the 160 billion tokens. We also demonstrate the *scalability* of the CRATE architecture by comparing the validation loss of CRATE and GPT-2 with respect to the model size in Figure 5 (*left*). Results show that the performance of CRATE is close to GPT-2 across all model sizes. However, we do recognize that forcing sparsification in a model potentially leads to a higher compute cost on the next-token-prediction objective, which aligns with observations in Bricken et al. [19] that *enabling monosemanticity might hurt model performance*. Analysis on the sparsity of CRATE and GPT-2 can be found in Appendix C.

Qualitative examples from CRATE and GPT-2 are demonstrated in Figure 5 (*right*). We conclude that CRATE can make reasonable predictions, encouraging us to further look into its neuron-level interpretability.

### 5.3. Interpretability

In order to quantitatively evaluate the interpretability of the neuron activations, we adopt the large language model-based algorithm introduced in Bills et al. [31] and Bricken et al. [19], as demonstrated in Algorithm 1. We retrieve the sparse code  $A_t$  (activations after the ReLU nonlinearity in the ISTA block) of CRATE for interpretation, and compare to activations from the MLP block of GPT-2.

In practice, we adopt three evaluation metrics: two from OpenAI (*top-and-random* and *random-only*) [31] and one from Anthropic [19]. We adopt the official implementation from Wu et al. [51], where details on the implementation are elaborated in Appendix B. Note that the Anthropic metric has much shorter text excerpts than the OpenAI metrics, so it is biased to sparse activations. For all evaluations, we discard the last layer of CRATE and GPT-2, according to the empirical observation that the last layer of CRATE is biased to the pre-training task [41].

---

**Algorithm 1** Interpretability Evaluation Algorithm [31]

---

- 1: **Inputs:** Input token set  $\mathcal{S}$  (in text form) and its activation matrix  $\mathbf{A} \in \mathbb{R}^{h \times T \times B}$  at  $\ell$ -th layer, where  $T$  is the length of a single text excerpt, and  $B$  is the number of text excerpts in the corpus.
  - 2: **Models:** Explanation model  $\mathcal{F}_1$ , simulation model  $\mathcal{F}_2$ .
  - 3: **for**  $i \in [d]$  **do**
  - 4:    $\mathbf{S}' \sim \mathcal{S}, \mathbf{A}' \in \mathbb{R}^{h \times T \times b} \sim \mathbf{A}$  : Retrieve  $b$  text excerpts of  $T$  tokens, together with the corresponding activation matrices.
  - 5:    $k_i = \mathcal{F}_1(\mathbf{S}', \mathbf{A}'_{i,*})$  : Explain common patterns in the retrieved activations of  $i$ -th neuron.
  - 6:    $\tilde{\mathbf{A}}'_{i,*} = \mathcal{F}_2(k_i, \mathbf{S}')$  : Use the explanation to simulate scores given only the tokens, not including true activations.
  - 7:    $\rho_i = \rho(\mathbf{A}'_{i,*}, \tilde{\mathbf{A}}'_{i,*})$  : Calculate correlation between the accurate and simulated activations.
  - 8: **end for**
  - 9: **Output:** Averaged interpretation score over all neurons  $\rho = \mathbb{E}_{i \in [d]}(\rho_i)$ .
- 

	Mean ( $\uparrow$ , darker green means more interpretable)						Variance ( $\downarrow$ , darker red means less steady)					
	Top-and-Random		Random-only		Anthropic		Top-and-Random		Random-only		Anthropic	
	CRATE	GPT-2	CRATE	GPT-2	CRATE	GPT-2	CRATE	GPT-2	CRATE	GPT-2	CRATE	GPT-2
1L	3.9	8.8	4.8	8.9	10.1	14.2	0.0	0.0	0.0	0.0	0.0	0.0
2L	8.05	4.2	6.95	1.95	11.35	10.2	0.06	0.01	1.1	0.12	0.0	0.25
3L	9.1	3.57	8.43	1.37	11.23	9.2	0.26	7.51	1.2	1.93	1.14	19.21
6L	7.96	5.4	6.36	3.14	10.4	8.52	2.29	20.85	1.87	18.39	2.01	32.56
12L	6.8	6.34	5.12	2.67	8.88	8.65	7.09	11.35	2.83	7.48	18.3	24.65

Table 2: Mean and variance of the average interpretability across layers for different model sizes.

**CRATE achieves markedly improved and more steady neuron-level interpretability across layers compared to GPT-2, applicable across a wide range of model sizes.** We show evaluation results of the interpretability of CRATE and GPT-2 averaged across layers in Table 2 (left). We observe that the interpretability of CRATE comprehensively outperforms GPT-2 on all metrics for  $L \in \{2, 3, 6, 12\}$ . When averaging the mean interpretability across all metrics, CRATE outperforms GPT-2 up to strikingly 103% relative improvement under the OpenAI Random-only metric when  $L = 6$ . We also present the layer-wise interpretation scores in Figure 6, which demonstrates that CRATE achieves higher interpretability than GPT-2 on almost all layers. For detailed distributions of the layer-wise scores of CRATE-Base compared to GPT2-Base on different metrics, refer to Appendix D.

The variances of the average interpretation scores of CRATE and GPT-2 across layers are shown in Table 2 (right). From the results we draw a solid conclusion that the interpretability of CRATE is much more steady than GPT-2 across all model sizes. Figure 6 further demonstrates a clear pattern that, for all model sizes, CRATE maintains a higher interpretability than GPT-2 among almost all layers.

**The built-in sparse coding approach introduces consistent and specific neuron-level behaviors.** The strong interpretability of CRATE on the OpenAI Top-and-Random metric and the Anthropic metric, as shown in Figure 6, indicates its consistent behavior on relevant tokens. These two methods contain a large portion of top-activated text excerpts, so they are valid for measuring whether the activations are consistent with the summarized explanation [19, 31]. Additionally, the larger interpretability gap of CRATE and GPT-2 on the OpenAI Random-only metric versus the Top-and-Random metric highlights the specificity of CRATE in avoiding firing on irrelevant tokens. The random-only metric usually includes highly irrelevant text excerpts, so it effectively measures the capability of the language model to avoid activating on semantically irrelevant tokens [31].

Qualitatively, we refer back to the interpretation examples shown in Figure 1. In this figure, we list three neurons from CRATE (row 1) and GPT-2 (row 2), respectively. For each neuron, we show two top-activated text excerpts and one random excerpt. Results show that CRATE is able to consistently activate on semantically similar tokens within the most relevant text excerpts, and does not activate on random tokens that are semantically distinguished from the top tokens. This promotes a more precise explanation given by the explanation model (Mistral in the figure). On the other hand, GPT-



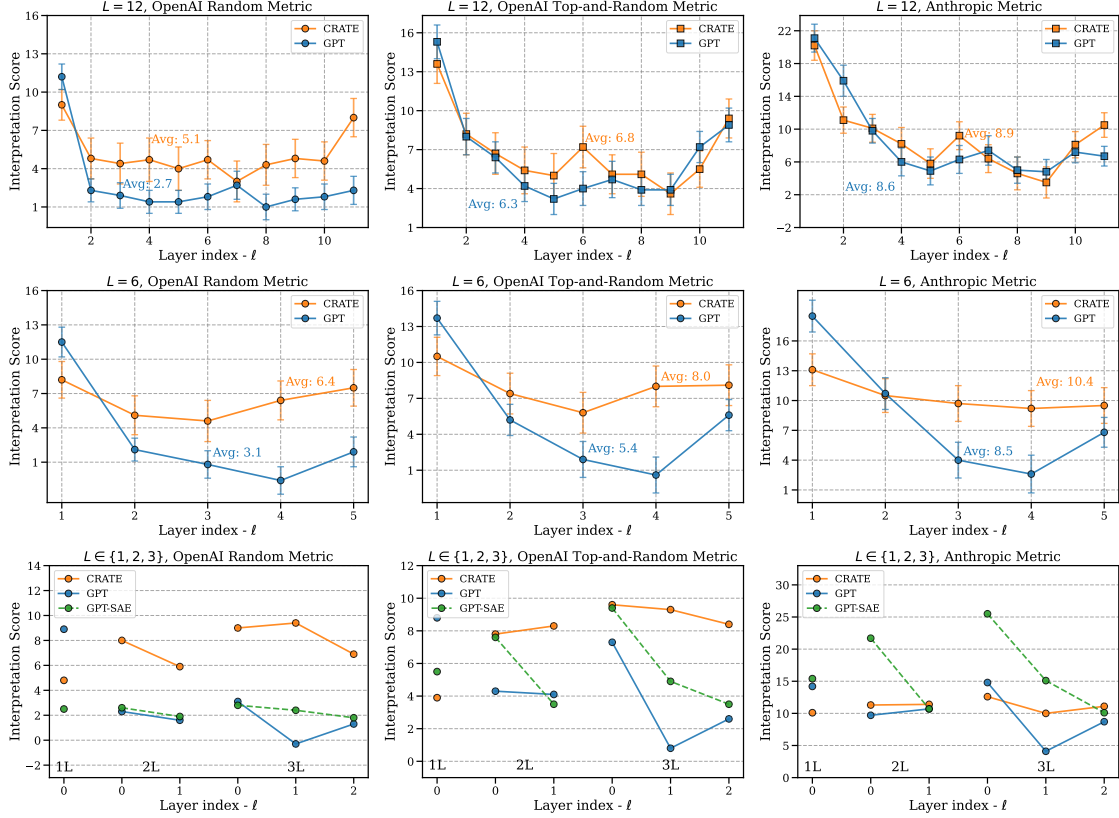


Figure 6: Interpretation scores evaluated using the OpenAI Random-only metric, Top-and-Random metric, and Anthropic metric, respectively. *Top*: interpretation scores of `CRATE` and GPT-2 for  $L = 12$ . *Middle*: interpretation scores of `CRATE` and GPT-2 for  $L = 6$ . *Bottom*: interpretation scores of `CRATE`, GPT-2, and GPT-2 with sparse auto-encoder for  $L \in \{1, 2, 3\}$ . Variance bars are normalized to 1/10 of its original size.

2 is much worse at distinguishing tokens from different contexts, because it also has high activations on random text excerpts where the semantic meanings deviate far from the top activations.

**Comparing CRATE to GPT-2 with post-hoc sparse auto-encoders.** We follow Bricken et al. [19] and train SAEs for models with layers  $L \in \{1, 2, 3\}$ , using output activations from GPT-2 on the Pile dataset’s training split, leading to the GPT2-SAE model. Details on the SAEs’ architecture and training are in Appendix E.

The interpretability scores of GPT2-SAE compared to `CRATE` and GPT-2, as depicted in Figure 6, reveal that under the long-context OpenAI metrics, GPT2-SAE matches GPT-2 but falls short of `CRATE`. This is attributed to its neuron activations becoming nearly 99% sparse after sparse auto-encoding, diminishing interpretability in long contexts. Conversely, under the Anthropic metric, GPT2-SAE surpasses both GPT-2 and `CRATE` in interpretability, corroborating findings in Bricken et al. [19] that post-hoc approaches enhance short-context interpretability, often a sign of mono-semanticity. However, the interpretability of GPT2-SAE on the Anthropic metric decreases significantly when  $\ell$  increases, while `CRATE` remains steady, introducing concern in scalability. Further qualitative comparisons can be found in Appendix F.

Besides its good performance on the Anthropic metric, the post-hoc dictionary learning approach requires considerable *manual effort*. To get a taste, training a sparse auto-encoder for a single GPT-2 layer takes 4 hours when  $h = 512$  and a day when  $h = 3072$  on an A100 GPU.



Figure 7: **Qualitative examples on logit effects of manually activating feature (i) in CRATE.** Text shown on the right side are the most positive changes in token prediction probability. The logit effects align with feature interpretations.

	OpenAI TaR	Anthropic
$\rho(\text{CRATE-}SAE) - \rho(\text{CRATE})$	-10.2	+34.8
$\rho(\text{GPT}_2\text{-}SAE) - \rho(\text{GPT}_2)$	+6.5	+38.1

Table 3: **Interpretability improvement of CRATE and GPT-2 after applying SAE.** Results are obtained by subtracting the interpretation scores of the language model and the SAE model trained on that language model.

**Does CRATE have more optimal representation than GPT-2 in terms of interpretability?** Alternatively, we train SAE models upon the CRATE model, denoted CRATE-SAE, and compare the interpretability improvement of CRATE-SAE over CRATE to the interpretability improvement of GPT2-SAE over GPT-2. As shown in Table 3, the improvement of interpretability of CRATE-SAE over CRATE is smaller than GPT2-SAE over GPT-2 under both OpenAI and Anthropic metrics. This suggests that CRATE has more optimal representations than GPT-2 in terms of interpretability. Experimental details can be found in Appendix E.5.

**Steering the CRATE model.** Following Bricken et al. [19], we manually activate some neurons and observe the *logit effects* (changes of the token probability of the language model head). Some qualitative examples are shown in Figure 7. Compared to the lossy steering of the SAE models, CRATE can be steered without loss. Discussions on the lossy steering process can be found in Appendix E.6.

#### 5.4. Ablation Study: Disentangling Interpretability from Other Factors

Despite the superior interpretability of CRATE, we’re interested in whether this interpretability comes from some side factors. Specifically, we’re interested in (i) whether it’s due to the worse performance of CRATE and (ii) whether it’s because CRATE has less parameters.

**Is the improved interpretability due to performance gap?** We first investigate whether the interpretability improvement is due to worse performance by comparing the interpretability of two different checkpoints of CRATE (intermediate checkpoint and full checkpoint). Results in Table 4 show that the interpretability of the intermediate checkpoint is lower than the full checkpoint, which suggests that “sacrificing” performance does *not* necessarily introduce better interpretation scores.

Checkpoint	Loss	0	1	2	3	4	5	6	7	8	9	10	Avg
79B Tokens	2.38	13.9	8.3	6.5	6.0	4.3	6.7	5.1	4.6	3.7	5.2	8.0	6.6
158B Tokens	2.29	13.6	8.2	6.7	5.4	5.0	7.2	5.1	5.1	3.6	5.5	9.4	6.8

Table 4: **Validation loss and interpretability of the CRATE model at different checkpoints.** The interpretation scores are measured under the OpenAI TaR metric.

Another piece of evidence is that CRATE-2L has higher interpretability scores than CRATE-1L. As shown in Figure 5 (left), CRATE-2L has much better performance than CRATE-1L on the next-token prediction task. On the other hand, as shown in Table 2, the interpretability of CRATE-2L is also much higher than CRATE-1L. Thus, a lower performance does not necessarily introduce higher interpretability.

**Is the interpretability gap due to number of parameters?** We observe that CRATE-Base (81.2M) has a similar number of parameters as GPT2-Small (81.1M). However, results in Table 2 indicate that the interpretability of CRATE-Base is higher than GPT2-Small on all metrics, and their layer-wise interpretation scores are also different in Figure 6. This evidence suggests that two models with similar number of parameters does not necessarily have similar interpretability.

Another piece of evidence is that the interpretability of CRATE/GPT2-1L all the way up to CRATE/GPT2-12L does not have a consistent trend of increasing/decreasing interpretability, but their number of parameters both monotonously increases. This indicates that a model with larger number of parameters does not necessarily has better/worse interpretability.

## 6. Conclusion, Limitation, and Future Work

In this paper, we demonstrated that replacing the standard transformer architecture with the white-box model CRATE as a foundational architecture significantly improves the interpretability. Our empirical findings on the capability of CRATE to be consistent and distinctive on the neuron-level activations underscore the importance of the white-box design in developing better language foundation models, fostering optimism that the introduction of built-in sparse coding approaches will catalyze further advancements in neuron-level interpretations.

Despite these findings, we acknowledge that the performance of CRATE is not as good as GPT-2 on the next-token prediction task, which is potentially due to the introduction of the ISTA operator that introduces sparsity. This aligns with previous work suggesting that the performance might drop when explicitly introducing sparsity [19]. Future work should investigate towards a better trade-off between performance and interpretability of language models with built-in sparsity. It would also be meaningful to research on more qualitative mechanisms in the white-box language model and how to use these mechanisms for downstream edits.

## References

- [1] Yoshua Bengio, Aaron Courville, and Pascal Vincent. Representation learning: A review and new perspectives. *IEEE transactions on pattern analysis and machine intelligence*, 35(8):1798–1828, 2013.
- [2] Jacob Devlin, Ming-Wei Chang, Kenton Lee, and Kristina Toutanova. BERT: Pre-training of Deep Bidirectional Transformers for Language Understanding. In Jill Burstein, Christy Doran, and Thamar Solorio, editors, *Proceedings of the 2019 Conference of the North American Chapter of the Association for Computational Linguistics: Human Language Technologies, NAACL-HLT 2019, Minneapolis, MN, USA, June 2-7, 2019, Volume 1 (Long and Short Papers)*, pages 4171–4186. Association for Computational Linguistics, 2019. doi: 10.18653/V1/N19-1423. URL <https://doi.org/10.18653/v1/n19-1423>.
- [3] Alec Radford, Jeffrey Wu, Rewon Child, David Luan, Dario Amodei, Ilya Sutskever, et al. Language models are unsupervised multitask learners. *OpenAI blog*, 1(8):9, 2019.
- [4] Ashish Vaswani, Noam Shazeer, Niki Parmar, Jakob Uszkoreit, Llion Jones, Aidan N Gomez, Łukasz Kaiser, and Illia Polosukhin. Attention is all you need. *Advances in neural information processing systems*, 30, 2017.
- [5] Tom B. Brown, Benjamin Mann, Nick Ryder, Melanie Subbiah, Jared Kaplan, Prafulla Dhariwal, Arvind Neelakantan, Pranav Shyam, Girish Sastry, Amanda Askell, Sandhini Agarwal, Ariel Herbert-Voss, Gretchen Krueger, Tom Henighan, Rewon Child, Aditya Ramesh, Daniel M. Ziegler, Jeffrey Wu, Clemens Winter, Christopher Hesse, Mark Chen, Eric Sigler, Mateusz Litwin, Scott Gray, Benjamin Chess, Jack Clark, Christopher Berner, Sam McCandlish, Alec Radford, Ilya Sutskever, and Dario Amodei. Language Models are Few-shot Learners. In Hugo Larochelle, Marc’Aurelio Ranzato, Raia Hadsell, Maria-Florina Balcan, and Hsuan-Tien Lin, editors, *Advances in Neural Information Processing Systems 33: Annual Conference on Neural Information Processing Systems 2020, NeurIPS 2020, December 6-12, 2020, virtual*, 2020. URL <https://proceedings.neurips.cc/paper/2020/hash/1457c0d6bfc4967418bfb8ac142f64a-Abstract.html>.
- [6] Long Ouyang, Jeffrey Wu, Xu Jiang, Diogo Almeida, Carroll Wainwright, Pamela Mishkin, Chong Zhang, Sandhini Agarwal, Katarina Slama, Alex Ray, et al. Training language models to follow instructions with human feedback. *Advances in Neural Information Processing Systems*, 35:27730–27744, 2022.
- [7] Patrick Lewis, Ethan Perez, Aleksandra Piktus, Fabio Petroni, Vladimir Karpukhin, Naman Goyal, Heinrich Küttler, Mike Lewis, Wen-tau Yih, Tim Rocktäschel, et al. Retrieval-augmented generation for knowledge-intensive nlp tasks. *Advances in Neural Information Processing Systems*, 33:9459–9474, 2020.
- [8] Jingfeng Yang, Hongye Jin, Ruixiang Tang, Xiaotian Han, Qizhang Feng, Haoming Jiang, Bing Yin, and Xia Hu. Harnessing the power of llms in practice: A survey on chatgpt and beyond. *arXiv preprint arXiv:2304.13712*, 2023.
- [9] Ziwei Ji, Nayeon Lee, Rita Frieske, Tiezheng Yu, Dan Su, Yan Xu, Etsuko Ishii, Ye Jin Bang, Andrea Madotto, and Pascale Fung. Survey of hallucination in natural language generation. *ACM Computing Surveys*, 55(12):1–38, 2023.
- [10] Shengbang Tong, Zhuang Liu, Yuexiang Zhai, Yi Ma, Yann LeCun, and Saining Xie. Eyes wide shut? exploring the visual shortcomings of multimodal llms. *arXiv preprint arXiv:2401.06209*, 2024.
- [11] Ismael Garrido-Muñoz, Arturo Montejo-Ráez, Fernando Martínez-Santiago, and L Alfonso Ureña-López. A survey on bias in deep nlp. *Applied Sciences*, 11(7):3184, 2021.

- [12] Moin Nadeem, Anna Bethke, and Siva Reddy. Stereoset: Measuring stereotypical bias in pre-trained language models. *arXiv preprint arXiv:2004.09456*, 2020.
- [13] Ronald Kemker, Marc McClure, Angelina Abitino, Tyler Hayes, and Christopher Kanan. Measuring catastrophic forgetting in neural networks. In *Proceedings of the AAAI conference on artificial intelligence*, 2018.
- [14] Yuexiang Zhai, Shengbang Tong, Xiao Li, Mu Cai, Qing Qu, Yong Jae Lee, and Yi Ma. Investigating the catastrophic forgetting in multimodal large language model fine-tuning. In *Conference on Parsimony and Learning*, pages 202–227. PMLR, 2024.
- [15] Chris Olah. Mechanistic interpretability, variables, and the importance of interpretable bases. *Transformer Circuits Thread*, page 2, 2022.
- [16] Kevin Meng, David Bau, Alex Andonian, and Yonatan Belinkov. Locating and editing factual associations in gpt. *Advances in Neural Information Processing Systems*, 35:17359–17372, 2022.
- [17] Zeyu Yun, Yubei Chen, Bruno A Olshausen, and Yann LeCun. Transformer visualization via dictionary learning: contextualized embedding as a linear superposition of transformer factors. *arXiv preprint arXiv:2103.15949*, 2021.
- [18] Kevin Meng, Arnab Sen Sharma, Alex Andonian, Yonatan Belinkov, and David Bau. Mass-editing memory in a transformer. *arXiv preprint arXiv:2210.07229*, 2022.
- [19] Trenton Bricken, Adly Templeton, Joshua Batson, Brian Chen, Adam Jermy, Tom Conerly, Nick Turner, Cem Anil, Carson Denison, Amanda Askell, et al. Towards monosemanticity: Decomposing language models with dictionary learning. *Transformer Circuits Thread*, page 2, 2023.
- [20] Connor Kissane. Attention saes scale to gpt-2 small. <https://www.lesswrong.com/posts/FSTRedtjuHa4Gfdbl/attention-saes-scale-to-gpt-2-small>, 2024.
- [21] Adly Templeton. *Scaling monosemanticity: Extracting interpretable features from claude 3 sonnet*. Anthropic, 2024.
- [22] Senthoran Rajamanoharan, Tom Lieberum, Nicolas Sonnerat, Arthur Conmy, Vikrant Varma, János Kramár, and Neel Nanda. Jumping ahead: Improving reconstruction fidelity with juprelu sparse autoencoders. *arXiv preprint arXiv:2407.14435*, 2024.
- [23] Yaodong Yu, Sam Buchanan, Druv Pai, Tianzhe Chu, Ziyang Wu, Shengbang Tong, Hao Bai, Yuexiang Zhai, Benjamin D Haeffele, and Yi Ma. White-box transformers via sparse rate reduction: Compression is all there is? *arXiv preprint arXiv:2311.13110*, 2023.
- [24] Hassan Sajjad, Nadir Durrani, and Fahim Dalvi. Neuron-level interpretation of deep nlp models: A survey. *Transactions of the Association for Computational Linguistics*, 10:1285–1303, 2022.
- [25] Yonatan Belinkov, Nadir Durrani, Fahim Dalvi, Hassan Sajjad, and James Glass. On the linguistic representational power of neural machine translation models. *Computational Linguistics*, 46(1):1–52, 2020.
- [26] Dumitru Erhan, Yoshua Bengio, Aaron Courville, and Pascal Vincent. Visualizing higher-layer features of a deep network. *University of Montreal*, 1341(3):1, 2009.
- [27] Nina Rimsky, Nick Gabrieli, Julian Schulz, Meg Tong, Evan Hubinger, and Alexander Matt Turner. Steering llama 2 via contrastive activation addition. *arXiv preprint arXiv:2312.06681*, 2023.
- [28] Evan Hernandez, Sarah Schwettmann, David Bau, Teona Bagashvili, Antonio Torralba, and Jacob Andreas. Natural language descriptions of deep visual features. In *International Conference on Learning Representations*, 2021.



- [29] Kenneth Kreutz-Delgado, Joseph F Murray, Bhaskar D Rao, Kjersti Engan, Te-Won Lee, and Terrence J Sejnowski. Dictionary learning algorithms for sparse representation. *Neural computation*, 15(2):349–396, 2003.
- [30] Arthur Conmy. My best guess at the important tricks for training 11 saes. <https://www.lesswrong.com/posts/fifPCos6ddsmJYahD/my-best-guess-at-the-important-tricks-for-training-11-saes>, 2023.
- [31] Steven Bills, Nick Cammarata, Dan Mossing, Henk Tillman, Leo Gao, Gabriel Goh, Ilya Sutskever, Jan Leike, Jeff Wu, and William Saunders. Language models can explain neurons in language models. URL <https://openaipublic.blob.core.windows.net/neuron-explainer/paper/index.html>. (Date accessed: 14.05. 2023), 2023.
- [32] Kevin Wang, Alexandre Variengien, Arthur Conmy, Buck Shlegeris, and Jacob Steinhardt. Interpretability in the wild: a circuit for indirect object identification in gpt-2 small. *arXiv preprint arXiv:2211.00593*, 2022.
- [33] Bilal Chughtai, Lawrence Chan, and Neel Nanda. A toy model of universality: Reverse engineering how networks learn group operations. In *International Conference on Machine Learning*, pages 6243–6267. PMLR, 2023.
- [34] Arthur Conmy, Augustine Mavor-Parker, Aengus Lynch, Stefan Heimersheim, and Adrià Garriga-Alonso. Towards automated circuit discovery for mechanistic interpretability. *Advances in Neural Information Processing Systems*, 36, 2024.
- [35] Yang Liu, Yuanshun Yao, Jean-Francois Ton, Xiaoying Zhang, Ruocheng Guo Hao Cheng, Yegor Klochkov, Muhammad Faaiz Taufiq, and Hang Li. Trustworthy llms: a survey and guideline for evaluating large language models’ alignment. *arXiv preprint arXiv:2308.05374*, 2023.
- [36] Collin Burns, Pavel Izmailov, Jan Hendrik Kirchner, Bowen Baker, Leo Gao, Leopold Aschenbrenner, Yining Chen, Adrien Ecoffet, Manas Joglekar, Jan Leike, et al. Weak-to-strong generalization: Eliciting strong capabilities with weak supervision. *arXiv preprint arXiv:2312.09390*, 2023.
- [37] Tom Lieberum, Matthew Rahtz, János Kramár, Geoffrey Irving, Rohin Shah, and Vladimir Mikulik. Does circuit analysis interpretability scale? evidence from multiple choice capabilities in chinchilla. *arXiv preprint arXiv:2307.09458*, 2023.
- [38] Nelson Elhage, Tristan Hume, Catherine Olsson, Nicholas Schiefer, Tom Henighan, Shauna Kravec, Zac Hatfield-Dodds, Robert Lasenby, Dawn Drain, Carol Chen, et al. Toy models of superposition. *arXiv preprint arXiv:2209.10652*, 2022.
- [39] Karol Gregor and Yann LeCun. Learning Fast Approximations of Sparse Coding. In Johannes Fürnkranz and Thorsten Joachims, editors, *Proceedings of the 27th International Conference on Machine Learning (ICML-10)*, June 21-24, 2010, Haifa, Israel, pages 399–406. Omnipress, 2010. URL <https://icml.cc/Conferences/2010/papers/449.pdf>.
- [40] Kwan Ho Ryan Chan, Yaodong Yu, Chong You, Haozhi Qi, John Wright, and Yi Ma. ReduNet: A White-box Deep Network from the Principle of Maximizing Rate Reduction. *Journal of Machine Learning Research*, 23(114):1–103, 2022. URL <http://jmlr.org/papers/v23/21-0631.html>.
- [41] Yaodong Yu, Tianzhe Chu, Shengbang Tong, Ziyang Wu, Druv Pai, Sam Buchanan, and Yi Ma. Emergence of segmentation with minimalistic white-box transformers. *arXiv preprint arXiv:2308.16271*, 2023.
- [42] Jinrui Yang, Xianhang Li, Druv Pai, Yuyin Zhou, Yi Ma, Yaodong Yu, and Cihang Xie. Scaling white-box transformers for vision. *arXiv preprint arXiv:2405.20299*, 2024.

- [43] Yi Ma, Harm Derksen, Wei Hong, and John Wright. Segmentation of Multivariate Mixed Data via Lossy Data Coding and Compression. *IEEE Trans. Pattern Anal. Mach. Intell.*, 29(9):1546–1562, 2007. doi: 10.1109/TPAMI.2007.1085. URL <https://doi.org/10.1109/TPAMI.2007.1085>.
- [44] Yaodong Yu, Kwan Ho Ryan Chan, Chong You, Chaobing Song, and Yi Ma. Learning Diverse and Discriminative Representations via the Principle of Maximal Coding Rate Reduction. In Hugo Larochelle, Marc’Aurelio Ranzato, Raia Hadsell, Maria-Florina Balcan, and Hsuan-Tien Lin, editors, *Advances in Neural Information Processing Systems 33: Annual Conference on Neural Information Processing Systems 2020, NeurIPS 2020, December 6-12, 2020, virtual*, 2020. URL <https://proceedings.neurips.cc/paper/2020/hash/6ad4174eba19ecb5fed17411a34ff5e6-Abstract.html>.
- [45] John Wright and Yi Ma. *High-Dimensional Data Analysis with Low-Dimensional Models: Principles, Computation, and Applications*. Cambridge University Press, 2022.
- [46] Victor Sanh, Lysandre Debut, Julien Chaumond, and Thomas Wolf. Distilbert, a distilled version of bert: smaller, faster, cheaper and lighter. *arXiv preprint arXiv:1910.01108*, 2019.
- [47] Leo Gao, Stella Biderman, Sid Black, Laurence Golding, Travis Hoppe, Charles Foster, Jason Phang, Horace He, Anish Thite, Noa Nabeshima, et al. The pile: An 800gb dataset of diverse text for language modeling. *arXiv preprint arXiv:2101.00027*, 2020.
- [48] Diederik P. Kingma and Jimmy Ba. Adam: A Method for Stochastic Optimization. In Yoshua Bengio and Yann LeCun, editors, *3rd International Conference on Learning Representations, ICLR 2015, San Diego, CA, USA, May 7-9, 2015, Conference Track Proceedings*, 2015. URL <http://arxiv.org/abs/1412.6980>.
- [49] Andrej Karpathy. nanoGPT. <https://github.com/karpathy/nanoGPT>, 2022.
- [50] Hugo Touvron, Thibaut Lavril, Gautier Izacard, Xavier Martinet, Marie-Anne Lachaux, Timothée Lacroix, Baptiste Rozière, Naman Goyal, Eric Hambro, Faisal Azhar, et al. Llama: Open and efficient foundation language models. *arXiv preprint arXiv:2302.13971*, 2023.
- [51] Jeff Wu, Hank Tillman, and Steven Bills. Automated interpretability. <https://github.com/openai/automated-interpretability>, 2023.
- [52] Arthur Conmy. sae. <https://github.com/ArthurConmy/sae>, 2024.

## A. Details on the CRATE Architecture

### A.1. Parameter Size of CRATE and GPT-2

CRATE is smaller than GPT-2 because of the architecture difference. The vanilla GPT-2 architecture has two main parameterized blocks: Attention block and MLP block.

**Parameter size of the MSSA Block.** In CRATE, the MSSA block resembles the Attention block, but instead of  $K, Q, V$  matrices, we only have one matrix. Therefore, compared to standard transformers, CRATE uses  $1/3$  of the parameters for the multi-head attention part.

**Parameter size of the ISTA block.** The MLP block in vanilla GPT-2 has one parametric matrix that transforms the input representations to the inner space (usually  $4\times$  larger), and another parametric matrix that transforms the inner representations back to the output space (as large as the input space). In CRATE, the MLP block is replaced by the overcomplete ISTA block, which transforms the input representation to the overcomplete basis ( $4\times$  larger) and transforms back with the same parametric matrix. Therefore, compared to standard transformers, CRATE uses  $1/2$  of the parameters for the MLP part.

### A.2. Causal MSSA Block

This process can be implemented by PyTorch-like code shown in Algorithm 2.

---

**Algorithm 2** PyTorch-Like Code for Causal MSSA Forward Pass

---

```
1 class CausalMSSA(nn.Module):
2     def __init__(self, config):
3         super().__init__()
4         assert config.n_embd % config.n_head == 0
5         self.c_attn = nn.Linear(config.n_embd, config.n_embd, bias=False)
6         self.c_proj = nn.Linear(config.n_embd, config.n_embd, bias=True)
7         self.attn_dropout = nn.Dropout(config.dropout)
8         self.resid_dropout = nn.Dropout(config.dropout)
9         self.n_head = config.n_head
10        self.n_embd = config.n_embd
11        self.dropout = config.dropout
12        self.register_buffer("bias", torch.tril(torch.ones(config.block_size, config.block_size)
13        ).view(1, 1, config.block_size, config.block_size)) # causal mask
14
15    def forward(self, x, enhanced_feature_id=None):
16        B, T, C = x.size()
17        qkv = qkv.view(B, T, self.n_head, C // self.n_head).transpose(1, 2)
18        att = (qkv @ qkv.transpose(-2, -1)) * (1.0 / math.sqrt(qkv.size(-1)))
19        att = att.masked_fill(self.bias[:, :, :T, :T] == 0, float('-inf'))
20        att = F.softmax(att, dim=-1)
21        att = self.attn_dropout(att)
22        y = att @ qkv
23        y = y.transpose(1, 2).contiguous().view(B, T, C)
24        y = self.resid_dropout(self.c_proj(y))
25        return y
```

---

### A.3. Overcomplete ISTA Block

To give a better idea of how Equation (9) works, we expand the two-iteration process ( $t = 2$ ). Given  $D^t \in \mathbb{R}^{d \times h}$ , we expand the first ISTA step to

$$\begin{aligned}
\mathbf{A}_0 &= \mathbf{0}, \\
\mathbf{A}_1 &= \mathcal{S}_\lambda \left( \mathbf{A}_0 - \eta \cdot (\mathbf{D}^\ell)^* (\mathbf{D}^\ell \mathbf{A}_0 - \text{LN}(\mathbf{Z}^{\ell+1/2})) \right) \\
&= \text{ReLU} \left( \eta \cdot (\mathbf{D}^\ell)^* \text{LN}(\mathbf{Z}^{\ell+1/2}) - \eta \lambda \right).
\end{aligned} \tag{10}$$

The second ISTA step continues the process from the initialized sparse code  $\mathbf{A}_1$ :

$$\begin{aligned}
\mathbf{A}_2 &= \mathcal{S}_\lambda \left( \mathbf{A}_1 - \eta \cdot (\mathbf{D}^\ell)^* (\mathbf{D}^\ell \mathbf{A}_1 - \text{LN}(\mathbf{Z}^{\ell+1/2})) \right) \\
&= \text{ReLU} \left( \mathbf{A}_1 - \eta \cdot (\mathbf{D}^\ell)^* (\mathbf{D}^\ell \mathbf{A}_1 - \text{LN}(\mathbf{Z}^{\ell+1/2})) - \eta \lambda \right),
\end{aligned} \tag{11}$$

which can be decomposed to:

$$\begin{aligned}
\mathbf{G}_1 &= (\mathbf{D}^\ell)^* \mathbf{D}^\ell \mathbf{A}_1 \\
\mathbf{G}_2 &= (\mathbf{D}^\ell)^* \cdot \text{LN}(\mathbf{Z}^{\ell+1/2}) \\
\mathbf{G} &= \eta \cdot (\mathbf{G}_2 - \mathbf{G}_1) - \eta \cdot \lambda \\
\mathbf{A}_2 &= \text{ReLU}(\mathbf{A}_1 + \mathbf{G})
\end{aligned} \tag{12}$$

where  $\mathbf{A}_2$  is the output sparse code. At last, we convert the output sparse code from the coding rate space back to the original representation space:

$$\mathbf{Z}^{\ell+1} = \mathbf{D}^\ell \mathbf{A}_2 \tag{13}$$

This process can be implemented by PyTorch-like code shown in Algorithm 3.

---

**Algorithm 3** PyTorch-Like Code for Over-complete ISTA Forward Pass

---

```

1 class ISTA(nn.Module):
2     def __init__(self, config):
3         super().__init__()
4         self.weight = nn.Parameter(torch.Tensor(4 * config.n_embd, config.n_embd)) # h*d
5         with torch.no_grad():
6             init.kaiming_uniform_(self.weight)
7         self.step_size = 0.1
8         self.lambd = 0.1
9
10    def forward(self, x, enhanced_feature_id=None):
11        z_init = F.relu(self.step_size * F.linear(x, self.weight, bias=None) - self.step_size *
12        self.lambd) # A1
13        x1 = F.linear(z_init, self.weight.t(), bias=None)
14        grad_1 = F.linear(x1, self.weight, bias=None)
15        grad_2 = F.linear(x, self.weight, bias=None)
16        grad_update = self.step_size * (grad_2 - grad_1) - self.step_size * self.lambd
17        output_sparse_code = F.relu(z_init + grad_update) # A2
18        output = F.linear(output_sparse_code, self.weight.t(), bias=None)
19        return output

```

---

#### A.4. Details of Processing Tokens

This section discusses the interpretation of Figure 3.

**In Figure 3, what is the space the points are drawn in?** The space is the representation space (of layer  $\ell$ ). Because the model is pretrained with next-token prediction in the language domain, the

space is specifically a semantic space. Thus, each point (token) has a semantic representation in this high-dimensional space.

**How do the layouts of the points suggest mono or poly-semanticity?** First, each axis (red/yellow) in the figure represents a neuron/feature visualized in the semantic space. We visualized the activation matrix  $A_t$  in Figure 8. For example, when  $L \in \{1, 2, 3\}$ , the model dimension is 128, which means that the overcomplete basis of ISTA will have a dimension of 512, introducing 512 features. Now if we input a sequence of 256 tokens, the activation matrix will have a shape of [512, 256].

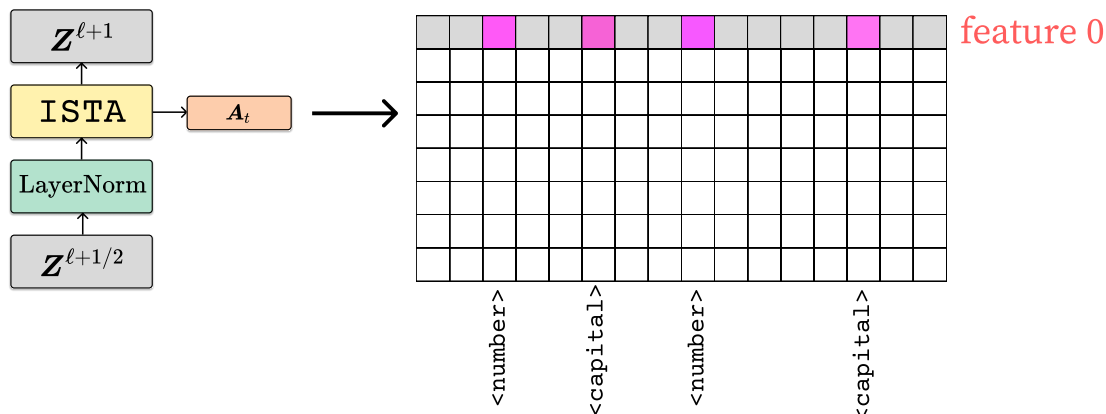


Figure 8: Illustration of the concepts of the activation matrix and poly-semanticity.

*Poly-semanticity* means that token representations in the semantic space are clustered as a broader set of semantic meanings, i.e., each neuron has a broader set of semantic meanings. For example, in the gray box on the top left of Figure 3, both yellow- and red-backgrounded tokens represent either a number or a capitalized token. This corresponds to multiple high activations in the feature, where the tokens that activated this feature can either be a number or a capitalized token, which is shown in Figure 8 (where pink squares represent high activations).

In the *compression* phase, the token representations are pushed towards the semantic axes, so that the tokens will activate on fewer features but will gain higher activations on these features, which is essentially an activation condensing process. In the *sparsification* phase, the neurons (axes) are made further from each other, meaning that the features have less semantic overlap with each other. In this case, the results will become the gray box on the top right side of Figure 3, indicating that each neuron has distinct semantic meanings, like “numbers” or “capitalized tokens”. Note that this is a minimal example. In practice, tokens appear in context.

## B. Details on Interpretability Evaluations

This section details the implementation details of the interpretability evaluations. In practice, we adopt three evaluation metrics: two from OpenAI [31] and one from Anthropic [19]. As the Anthropic metric is a closed-source follow-up of OpenAI, we start from the official implementation provided by OpenAI [51] for both metrics. For each layer, we use randomly sampled 8,000 text excerpts of 1,024 tokens each, which sums up to 8M tokens in total, from the test split of the uncopyrighted Pile dataset, to evaluate the interpretability scores.

### B.1. Parameters of Evaluation Metrics

Comprehensive parameter settings are shown in Table 5. For the OpenAI metrics, each input text excerpt contains 64 tokens. For the *OpenAI top-and-random* metric, we use 5 top activated excerpts for explanation, and a mixture of 5 top activated and 5 randomly activated excerpts for simulation. For the *OpenAI random-only* metric, we only use 5 randomly activated excerpts for simulation.



For the *Anthropic* metric, each text excerpt contains only 8 tokens. For the explanation model, we input 15 top activated excerpts, 5 randomly activated excerpts, and 22 excerpts from different activation quantiles. To elaborate, we evenly divide the activation range into 11 quantiles, where we pick 2 excerpts from each of them. For the simulation model, we input 10 top activated excerpts, 5 randomly activated excerpts, 22 quantiled excerpts, and 10 top activated out-of-context (OOC) excerpts. Our implementation of the OOC excerpts is to cut the input text excerpt into length of only 3 tokens.

Table 5: Evaluation parameter settings of the OpenAI and Anthropic approach.

		Explanation				Simulation			
		#Token	#Top	#Rand	#Qua	#Top	#Rand	#Qua	#OOC
<b>OpenAI</b>	TaR	64	5			5	5		
	Rand	64	5				5		
<b>Anthropic</b>		8	15	5	2 · 11	10	5	2 · 11	10

## B.2. Discussion on Focus of Different Measures

The OpenAI random-only metric is the easiest to interpret. As noted by Bills et al. [31], the random-only metric considers an explanation’s ability to capture the neuron’s representation of features in the pre-training distribution, because the simulated tokens are uniformly randomly sampled from the validation set of the pre-train dataset. However, the random-only scoring with small sample size risks failing to capture behavior, due to lacking both tokens with high simulated activations and tokens with high real activations. Top-and-random scoring addresses the latter, but causes us to penalize falsely low simulations more than falsely high simulations, and thus tends to accept overly broad explanations.

The Anthropic metric, on the other hand, puts more focus on the mono-semanticity of the activations, as noted by Bricken et al. [19]. For sparse features, which don’t fire on most random samples, evaluating across a wide range of activations effectively tests the model’s ability to distinguish a feature’s large activations from zero, and the short text excerpts make it easier for the simulation model to identify the sparse activations.

## B.3. More Accessible Evaluation

To reduce compute cost, we use `Mistral-7B-instruct` as the explanation model, and `LLaMA-2-7B` as the simulation model. We empirically prove that these replacements does not affect the conclusions of apple-to-apple comparison between `CRATE` and `GPT-2` below.

**Explanation model.** In the official implementation [51], the explanation model is `gpt-4`. According to ablations described in Bills et al. [31], it also makes sense to use the slightly cheaper model `gpt-3.5-instruct`. Due to the high compute cost, we use the open-source model `mistral-7b-instruct` instead. We demonstrate the performance of `gpt-3.5-turbo` and `mistral-7b-instruct` using the OpenAI random-only and top-and-random metrics in Table 6. Results show that the change of model doesn’t significantly change the scores, and doesn’t affect conclusions at all.

**Simulation model.** The official implementation of the simulation model utilizes `text-davinci-003` (now named `gpt-3.5-turbo-instruct`), which no longer supports retrieving the logprobs through the API, so we use `LLaMA-2-70B` as an equally capable replacement [50]. For more accessible evaluations, we use `LLaMA-2-7B` instead. We show the difference in interpretability caused by different simulation model size on `LLaMA-2-7B` and `LLaMA-2-70B` in Table 7. Empirical results show that although `LLaMA-2-7B` has overall lower scores and higher variance than `LLaMA-2-70B`, it doesn’t affect essential conclusions about the apple-to-apple comparison between `CRATE` and `GPT-2`.

Table 6: Interpretability measure of GPT-2, GPT2-SAE and CRATE on the Pile dataset based on the OpenAI metrics. Explanation model: Mistral-7B-instruct/GPT-3.5-turbo. Simulation model: LLaMA-2-7B.

mistral-7b-instruct			$\rho$ (Random-only) (% , $\uparrow$ )			$\rho$ (Top-and-Random) (% , $\uparrow$ )		
Model	Size	Loss	Layer 1	Layer 2	Layer 3	Layer 1	Layer 2	Layer 3
CRATE-1L	6.54M	4.06	4.8	-	-	3.9	-	-
CRATE-2L	6.64M	3.55	8.0	5.8	-	7.8	8.3	-
CRATE-3L	6.74M	3.46	9.0	9.4	6.9	9.6	9.3	8.4
GPT-1L	6.64M	3.83	8.9	-	-	8.8	-	-
GPT-2L	6.83M	3.23	2.3	1.6	-	4.3	4.1	-
GPT-3L	7.03M	3.11	3.1	-0.3	1.3	7.3	0.8	2.6
GPT-1L (16x SAE)			2.9	-	-	5.4	-	-
GPT-2L (16x SAE)			3.5	1.8	-	7.4	4.2	-
GPT-3L (16x SAE)			3.2	2.3	1.1	9.6	5.0	4.5

GPT-3.5-turbo			$\rho$ (Random-only) (% , $\uparrow$ )			$\rho$ (Top-and-Random) (% , $\uparrow$ )		
Model	Size	Loss	Layer 1	Layer 2	Layer 3	Layer 1	Layer 2	Layer 3
CRATE-1L	6.54M	4.06	4.8	-	-	3.9	-	-
CRATE-2L	6.64M	3.55	8.2	6.0	-	7.5	8.0	-
CRATE-3L	6.74M	3.46	9.1	9.2	6.9	9.5	9.1	8.3
GPT-1L	6.64M	3.83	9.0	-	-	9.0	-	-
GPT-2L	6.83M	3.23	2.2	1.6	-	4.3	4.4	-
GPT-3L	7.03M	3.11	3.0	-0.3	1.2	7.0	3.1	3.0
GPT-1L (16x SAE)			2.6	-	-	4.7	-	-
GPT-2L (16x SAE)			3.4	1.6	-	5.0	2.9	-
GPT-3L (16x SAE)			2.8	1.8	1.2	7.4	3.8	3.2

Table 7: Interpretability measure of GPT-2 and CRATE on the Pile dataset based on the OpenAI Top-and-random metric. Explanation model: GPT-3.5-turbo. Simulation model: LLaMA-2-7B/LLaMA-2-70B.

	Interpretability (7B) (% , $\uparrow$ )			Interpretability (70B) (% , $\uparrow$ )		
	Layer 1	Layer 2	Layer 3	Layer 1	Layer 2	Layer 3
CRATE-1L	3.9	-	-	6.4	-	-
CRATE-2L	7.5	8.0	-	7.4	7.1	-
CRATE-3L	9.5	9.1	8.3	10.4	7.4	6.5
GPT-1L	9.0	-	-	13.4	-	-
GPT-2L	4.3	4.4	-	6.4	7.8	-
GPT-3L	7.0	3.1	3.0	10.1	3.2	6.3

		Layer 1	Layer 2	Layer 3	Layer 4	Layer 5	Layer 6
<b>7B</b>	CRATE-6L	10.5	7.4	5.8	8.0	8.1	5.7
	GPT-6L	13.7	5.2	1.9	0.6	5.6	6.9
<b>70B</b>	CRATE-6L	10.1	6.5	7.0	8.3	9.4	0.7
	GPT-6L	14.5	6.2	2.5	0.7	3.9	4.1

### C. Analysis on Activation Sparsity

We demonstrate the activation sparsity of CRATE compared to GPT-2 in Figure 9. One might have the confusion about why CRATE is designed to be sparse but the activations evaluated is denser than GPT-2. Note that the sparsity evaluated in standard transformer model is output from the hidden layer of the MLP layer, which is the activation matrix  $A$  before applying to the residual stream, as shown in Figure 10. The actual representations in standard transformers, which are after applying the residual stream, are not sparse at all. In contrast, the sparsity evaluated in CRATE is the actual representations  $A_t$  (including the residual stream).

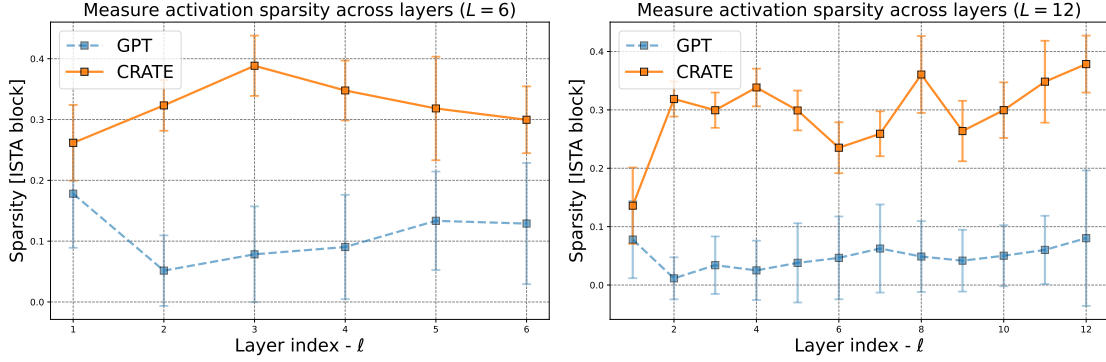


Figure 9: Layer-wise activation sparsity of CRATE and GPT. *Left*: 6L models. *Right*: 12L models.

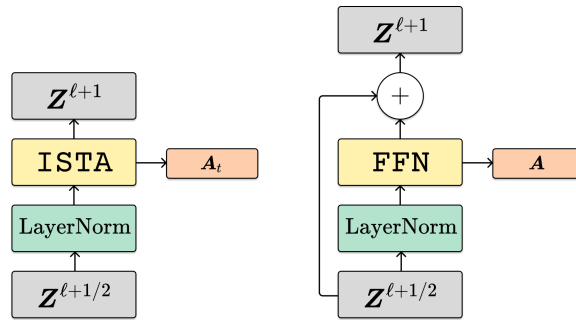


Figure 10: Extracting sparse code  $A_t$  from CRATE and hidden layer output  $A$  from GPT-2.

We also present the activation dynamics of CRATE and GPT-2 with the progression of the pre-training process in Figure 11. We observe a strong trend that the sparsity of CRATE monotonically decreases in the early stage (trained on 1.6B tokens), which aligns with the design purpose. In the late stage (16B, 160B tokens), the sparsities in the early sites ( $L < 12$ ) significantly decreases, which also aligns with the design purpose. On the other hand, GPT-2 never appears to have a decreasing trend of activation sparsity over layers across the whole pre-training stage, indicating a systematic difference between the sparsity dynamics between CRATE and GPT-2. One counter-intuitive observation is that the decreasing trend fades as the stage moves on. Our hypothesis is that CRATE overfits on the next token prediction task due to the large amount of tokens trained.

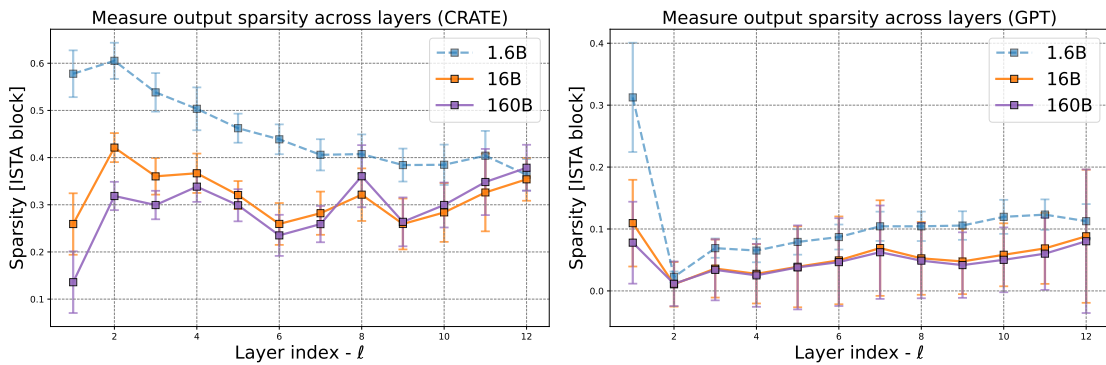


Figure 11: Layer-wise activation sparsity w.r.t. tokens trained. *Left*: CRATE language model. *Right*: GPT-2.

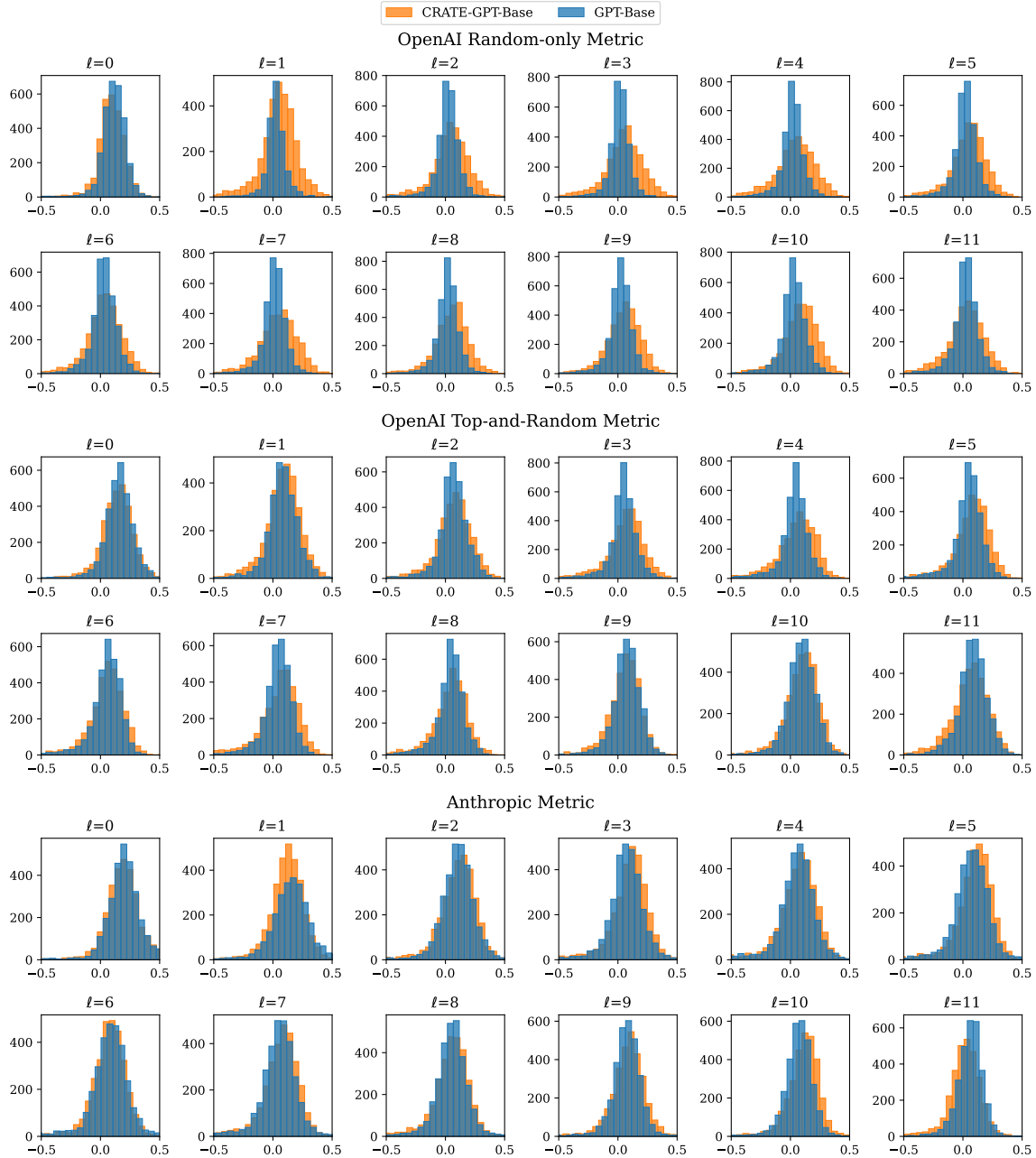


Figure 12: Distribution of the interpretation scores over CRATE-12L and GPT2-12L.  $x$ -axis: interpretation score.  $y$ -axis: count of neurons falling in the corresponding interval of interpretation score.

## D. Details on Interpretation Score Distributions

We visualize the distributions of layer-wise interpretation scores of CRATE and GPT-2 with  $L = 12$  in Figure 12. We exclude cases where activations sampled from GPT2-Base (random-only metric) are all zeroes, as in these cases the correlation  $\rho$  will be undefined. This results in a smaller number counted in the GPT-2 activations in the first two rows.

## E. Details on Sparse Auto-encoder

### E.1. Sparse Autoencoder and Dictionary Learning

The dictionary learning model is an MLP model with a single hidden layer. It is trained as an auto-encoder using input weights as the encoder (which maps the input activations to a higher dimension), and output weights as the decoder. Formally, given activation  $\mathbf{a} \in \mathbb{R}^h$  sampled from  $\mathbf{A} \in \mathbb{R}^{h \times N}$ , the encoder  $\mathbf{W}_1, \mathbf{b}_1$  with dimension multiplier  $\mu$  maps the activations to a hidden representation  $\mathbf{h} \in \mathbb{R}^{\mu h}$ , whereas the decoder  $\mathbf{W}_2, \mathbf{b}_2$  maps the representation back to the original dimension  $\hat{\mathbf{a}} \in \mathbb{R}^h$ . The dictionary learning objective can thus be expressed as

$$\bar{\mathbf{a}} = \mathbf{a} - \mathbf{b}_2 \quad (14)$$

$$\mathbf{h} = \text{ReLU}(\mathbf{W}_1 \bar{\mathbf{a}} + \mathbf{b}_1) \quad (15)$$

$$\hat{\mathbf{a}} = \mathbf{W}_2 \mathbf{h} + \mathbf{b}_2 \quad (16)$$

$$\mathcal{L} = \frac{1}{|\mathbf{A}|} \sum_{\mathbf{a} \in \mathbf{A}} \|\mathbf{a} - \hat{\mathbf{a}}\|_2^2 + \lambda \|\mathbf{h}\|_1 \quad (17)$$

### E.2. Detailed Setup

We train the sparse auto-encoders on the train split of the uncopyrighted Pile dataset until convergence. Following Bricken et al. [19] and Conmy [30], we adopt the resampling strategy to re-train the dead features, and the learning rate scheduling strategy to improve recovery rate. For implementation, we mainly follow Conmy [52], with  $\lambda_{\ell_1} = 1.6 \times 10^{-4}$ ,  $\alpha = 1.2 \times 10^{-3}$  for all sizes of models. We evaluate using the average loss of randomly sampled batches on the validation split of the uncopyrighted Pile dataset.

### E.3. Loss Curve

The loss curves of training the sparse auto-encoders are shown in Figure 13. Generally, resampling boosts the performance of the recovery score, which aligns with the conclusions shown in Bricken et al. [19] and [30]. We also observe an increasing trend of performance with the increases of the SAE multiplication factor  $\mu$  and model size  $L$ .

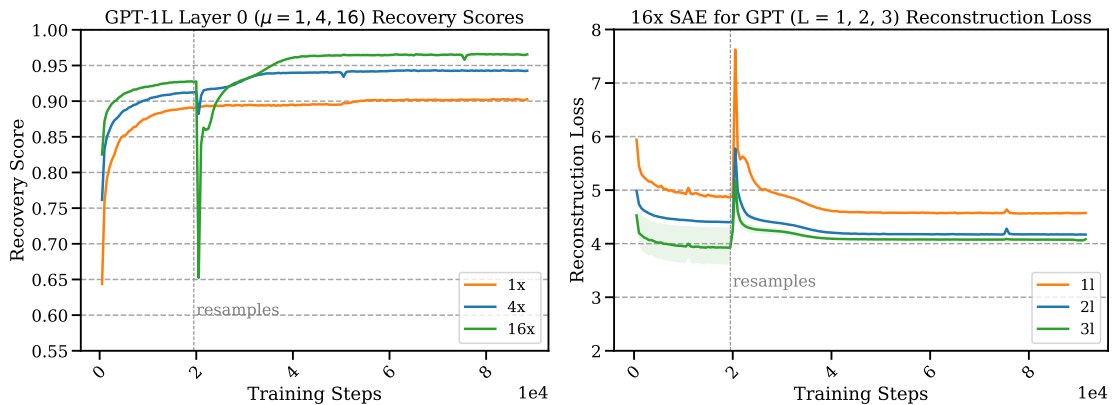


Figure 13: *Left:* The recovery scores of GPT-1L ( $\ell = 0$ ) with SAE multiplication factors  $\mu \in \{1, 4, 16\}$ . *Right:* The reconstruction loss of SAE with  $\mu = 16$  on different sizes of GPT-2 models  $L \in \{1, 2, 3\}$ , averaged across all layers.



## E.4. Performance

The performance of sparse auto-encoders of CRATE and GPT-2 under a variety of settings (model  $L, \ell$  and sparse autoencoder width multiplication factor  $\mu$ ) are shown in Table 8. The percentages of dead neurons for all layers of  $L \in \{1, 2, 3\}$  are less than 1%.

Table 8: Reconstruction loss and recovery score of the sparse autoencoders on CRATE and GPT-2.

$\mu = 16$			Reconstruction Loss ( $\downarrow$ )			Recovery Score ( $\%, \uparrow$ )		
	Size	Loss	Layer 0	Layer 1	Layer 2	Layer 0	Layer 1	Layer 2
GPT-1L	6.64M	3.83	4.35	-	-	95.0	-	-
GPT-2L	6.83M	3.23	3.50	3.45	-	95.2	92.2	-
GPT-3L	7.03M	3.11	3.38	3.39	3.29	94.6	94.8	92.4
CRATE-1L	6.54M	4.06	4.33	-	-	93.6	-	-
CRATE-2L	6.64M	3.55	4.12	3.80	-	95.7	95.7	-
CRATE-3L	6.74M	3.46	4.05	3.99	3.77	93.0	93.9	95.0
$\mu = 4$			Reconstruction Loss ( $\downarrow$ )			Recovery Score ( $\%, \uparrow$ )		
	Size	Loss	Layer 0	Layer 1	Layer 2	Layer 0	Layer 1	Layer 2
GPT-1L	6.64M	3.83	4.34	-	-	93.7	-	-
GPT-2L	6.83M	3.23	3.59	3.56	-	92.7	88.6	-
GPT-3L	7.03M	3.11	3.45	3.50	3.34	92.2	94.9	89.9
CRATE-1L	6.54M	4.06	4.39	-	-	92.1	-	-
CRATE-2L	6.64M	3.55	4.37	3.93	-	93.7	93.8	-
CRATE-3L	6.74M	3.46	4.03	4.11	3.81	92.6	92.6	92.6
$\mu = 1$			Reconstruction Loss ( $\downarrow$ )			Recovery Score ( $\%, \uparrow$ )		
	Size	Loss	Layer 0	Layer 1	Layer 2	Layer 0	Layer 1	Layer 2
GPT-1L	6.64M	3.83	4.93	-	-	95.0	-	-
GPT-2L	6.83M	3.23	3.89	3.75	-	89.0	82.2	-
GPT-3L	7.03M	3.11	3.63	3.61	3.58	86.9	91.0	84.9
CRATE-1L	6.54M	4.06	4.69	-	-	86.2	-	-
CRATE-2L	6.64M	3.55	4.68	4.29	-	90.4	88.9	-
CRATE-3L	6.74M	3.46	4.39	4.38	4.16	97.0	89.2	88.1

## E.5. Interpretability

In Section 5.4, we’ve demonstrated that CRATE has more optimal representation than GPT-2 in terms of interpretability. Here we show the details of this experiment and layer-wise decomposition of the interpretability comparison shown in Table 3.

As it’s hard to decide how much interpretability gain it is from CRATE to CRATE-SAE directly (as explained in Section 5.3), we compare the interpretability *improvement* of CRATE-SAE over CRATE to the interpretability improvement of GPT2-SAE over GPT-2. The interpretability of GPT2-SAE is already included in Figure 6. The interpretability of CRATE-SAE under the OpenAI TaR and Anthropic metrics are shown in Table 9.

Table 9: Interpretability of CRATE-SAE under the OpenAI TaR and Anthropic metrics.

	OpenAI TaR ( $\uparrow$ )			Anthropic ( $\uparrow$ )		
	Layer 1	Layer 2	Layer 3	Layer 1	Layer 2	Layer 3
1L	6.0	-	-	17.9	-	-
2L	7.7	5.2	-	21.7	12.4	-
3L	7.2	6.4	4.6	19.3	18.4	11.6

## E.6. Steering the LM or SAE

In comparison to post-hoc trained SAEs, built-in sparsification processes, such as the one we proposed in this paper, have the potential to be steered with perfect fidelity. As visualized in Figure 14, post-hoc approaches like SAE require steering the model with the decomposed hidden states  $h$ , whose encoding and decoding processes are both *lossy*. An imperfect reconstruction systematically leads to *distortions* of the steering signal upon the hidden states, and thus affects downstream applications of the GPT2-SAE model. In contrast, CRATE doesn't include any approximation that distorts the steering signal, so the signal can be propagated without loss of fidelity. This conclusion does not change whether the performance of GPT2-SAE outperforms CRATE or not.

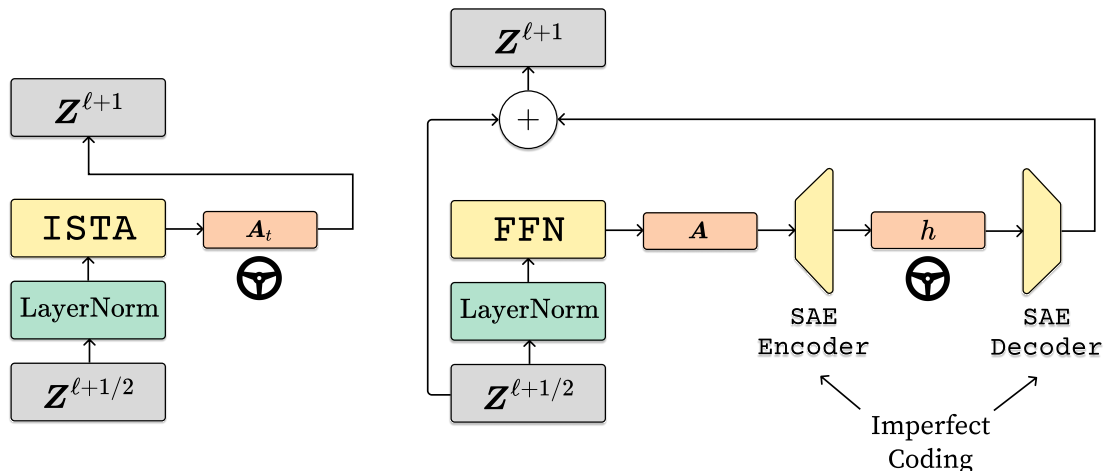


Figure 14: Illustration of steering a language model directly or using SAE.

## F. Further Qualitative Results on Interpretable Neurons

This section lists some further qualitative examples of tokens and their activations when  $L = 3$ , including examples of the GPT2-SAE activations. Specifically, we demonstrate two neurons in each model. Tokens with a deeper blue background have a higher activation. Explanations  $k_i$  and scores  $s_i$  are obtained by Algorithm 1.

### F.1. CRATE-3L, Layer 0, Neuron 288

**OpenAI Evaluation Score:** 0.44478400135318646

**Explanation:** information related to the regulation of mRNA expression and its role in carbohydrate metabolism, with a focus on CRC cells and gene signaling in the context of cancer development.

#### Top Activations

animal models of cartilage degradation ([@b41-mm r-16-04-3841]). Among these cytokines, IL-1 $\beta$  is highly overexpressed in the cartilage and in the synovial tissue, while the expression of IL-1 receptor antagonist ([@b42-mm r-rafts. Moreover, AC OX1 overexpression attenuated the augmentation of migration and invasion of CRC cells by mi R-15 b-5 p overexpression. In conclusion, our study demonstrated a functional role of the SIRT1 / mi R-15 b-5 p / AC OX1 axis

#### Random Activations

ed with Peter Braun, the Moravian mission ary in Antigua; and to that correspondence he owed in part his interest in missionary work. But that was not the end of the Brethren's influence. At all meetings addressed by the founders of the proposed Society, the speaker repeatedly

ESA) and the American Association for the Advancement of Science (AAAS) have well-developed and successful science policy fellows programs. These programs acknowledge that scientists can play important roles in directing new laws and policies in their field, and that their expertise is needed for effective decision-making \

**Anthropic Evaluation Score:** 0.2813215497394413

**Explanation:** Phrases related to molecular biology and gene expression, specifically in the context of mRNA transcription and its activation or inhibition. Additionally, there are mentions of certain proteins (IPOTENT, cytokine, IRT), cellular processes (proliferation,

**Top Activations**

b-5p overexpression.  
 cases showed EGFR overexpression.  
 , TLR2 overexpression in  
 IL-1 $\beta$  mRNA expression in the

**Random Activations**

G. albidus \* TMW  
 had suffered from heat contact urticaria  
 "alive": true, \n  
 = \_mm\_pack us \_ ep

**F.2. GPT-3L, Layer 2, Neuron 289**

**OpenAI Evaluation Score:** -0.3236237946813878

**Explanation:** The provided text contains multiple sections, but the activations given for Neuron 4 seem to be related to genetic and statistical data (e.g., population, CI, percent, risk association, and recessive models). Given this, the main thing this neuron does is identify

**Top Activations**

in Asian population. Similarly, in Caucasian population, the rs499776 polymorphism attributes risk association in homozygote OR 0.70 (95% CI [0.50-0.98]), dominant OR 3.57 (95% CI [2.34-5.27]), and recessive models OR 0  
 \*SE\* = 0.0440, \*t\* = -1.0775, \*p\* > 0.05, 95% CI (-0.1338, 0.0390) for the Slovakian villagers story\], therefore indicating full mediation by exonerations and out-group focused emotions

**Random Activations**

longer the vortex, it's the smooth current of rotating air which is next to \n the vortex, and we use the updraft of this air." Taking advantage of the free \n lift in this updraft of air is called "wake-energy retrieval." ... on long-\n haul flights, fuel savings of between  
 ushing.\n\n Sigh called her supervisor. Sergeant Sweeney and Deputy Ray responded \n \n and moved Donery so that Sigh could search his cell. Donery had been in his new \n \n cell for less than five minutes when the toilet overflowed and water began flowing out \n \n of

**Anthropic Evaluation Score:** 0.06532542667915378

**Explanation:** strings containing specific numbers and alphanumeric characters, such as "CI-50-", "e-44-", "87-", and "f-". Additionally, it activates slightly for certain words like "cost", "weeks", "disability", and

**Top Activations**

95% CI [0.50-  
 95% CI, 0.13-  
 f\], [0.2222  
 95% CI [0.50-

**Random Activations**

{8}{45}\pi \n  
 instead of that silly website. <|endoftext|>How

is free software ; you can redistribute

### F.3. GPT-3L-SAE-16x, Layer 2, Neuron 57

**OpenAI Evaluation Score:** 0.1427145260798203

**Explanation:** months or the word "Bank" followed by a year.

**Top Activations**

No . 18 - 20 609 February 21 , 2020 \n

with the compact - open topology , is a locally compact group . ' \n author : \n - ' Nicolas Radu [ ^ 1 ] ' \n date : ' July 15 , 2016 ' \n title : | \n A topological characterization of the Moufang \n property for compact polygons

**Random Activations**

of DN \* db / db \* mice . \n ( \*\* A \*\* ) Urinary albumin to creatinine ratio . ( \*\* B \*\* ) Serum urea nitrogen . ( \*\* C \*\* ) Left kidney weight to body weight ratio . ( \*\* D \*\* ) HE staining . Bar =

this email : otisdarko60@yahoo.com \n \n HE FIX THE FOLLOWING PROBLEMS TO ALL \n \n ACROSS THE GLOBE ON : \n \n 1 . Getting your lover or husband back \n \n 2 . Spiritual bullet proof \n \n 3 . Training \n \n 4 . Money

**Anthropic Evaluation Score:** 0.2540425061001668

**Explanation:** dates and specifically, the month and day for a given year. The neuron is not activated by the year alone, and it requires both the month and day for a complete activation.

**Top Activations**

February 21 , 2020

\n date : ' July 15 , 2016

field , Missouri ( December 15 , 2014

February 5 , 1998

**Random Activations**

\n Canola oil

} \n \n .cke

uana when a draw would have clinched

. < / p > \n \t